



Review

Polybenzimidazole-Based Polymer Electrolyte Membranes for High-Temperature Fuel Cells: Current Status and Prospects

Zhengping Zhou ¹, Oksana Zholobko ¹ , Xiang-Fa Wu ^{1,*}, Ted Aulich ^{2,*}, Jivan Thakare ²  and John Hurley ²

¹ Department of Mechanical Engineering, North Dakota State University, Fargo, ND 58108, USA; milozhengping@gmail.com (Z.Z.); Oksana.Zholobko@ndsu.edu (O.Z.)

² Energy & Environmental Research Center, University of North Dakota, Grand Forks, ND 58202, USA; jthakare@undeerc.org (J.T.); jhurley@undeerc.org (J.H.)

* Correspondence: xiangfa.wu@ndsu.edu (X.-F.W.); taulich@undeerc.org (T.A.); Tel.: +1-701-231-8836 (X.-F.W.); Fax: +1-701-231-8913 (X.-F.W.)

Abstract: Polymer electrolyte membrane fuel cells (PEMFCs) expect a promising future in addressing the major problems associated with production and consumption of renewable energies and meeting the future societal and environmental needs. Design and fabrication of new proton exchange membranes (PEMs) with high proton conductivity and durability is crucial to overcome the drawbacks of the present PEMs. Acid-doped polybenzimidazoles (PBIs) carry high proton conductivity and long-term thermal, chemical, and structural stabilities are recognized as the suited polymeric materials for next-generation PEMs of high-temperature fuel cells in place of Nafion[®] membranes. This paper aims to review the recent developments in acid-doped PBI-based PEMs for use in PEMFCs. The structures and proton conductivity of a variety of acid-doped PBI-based PEMs are discussed. More recent development in PBI-based electrospun nanofiber PEMs is also considered. The electrochemical performance of PBI-based PEMs in PEMFCs and new trends in the optimization of acid-doped PBIs are explored.



Citation: Zhou, Z.; Zholobko, O.; Wu, X.-F.; Aulich, T.; Thakare, J.; Hurley, J. Polybenzimidazole-Based Polymer Electrolyte Membranes for High-Temperature Fuel Cells: Current Status and Prospects. *Energies* **2021**, *14*, 135. <https://doi.org/10.3390/en14010135>

Received: 25 November 2020

Accepted: 22 December 2020

Published: 29 December 2020

Publisher's Note: MDPI stays neutral with regard to jurisdictional claims in published maps and institutional affiliations.



Copyright: © 2020 by the authors. Licensee MDPI, Basel, Switzerland. This article is an open access article distributed under the terms and conditions of the Creative Commons Attribution (CC BY) license (<https://creativecommons.org/licenses/by/4.0/>).

Keywords: fuel cells; polymer electrolyte membranes; proton exchange membranes (PEMs); polybenzimidazole (PBI); high-temperature PEMs; acid doping; proton conductivity; nanofibers

1. Introduction

Fuel cells, as attractive energy-conversion devices, are able to directly convert chemical energy stored in hydrogen and other simple organic substances into electrical energy via an electrochemical reaction. The energy conversion efficiency in fuel cells is up to 60%, much higher than those of conventional combustion-based power plants (~33%) and internal combustion engines installed in today's ground vehicles (~20%). More importantly, fuel cells only produce pollution-free emissions, pure water, and potentially reusable heat. Together, these features strongly suggest that fuel cells not only address the major problems associated with the production and consumption of energies but also meet the increasing societal and environmental needs [1]. To date, several types of fuel cells have been developed, including alkaline fuel cells (AFCs), polymer electrolyte membrane fuel cells (PEMFCs), phosphoric acid fuel cells (PAFCs), molten carbonate fuel cells (MCFCs), and solid-oxide fuel cells (SOFCs) [2–4]. Among various types of fuel cells, PEMFCs are widely regarded as the most promising for light-duty transportation and portable energy applications. PEMFCs possess several attractive advantages, such as high energy efficiency, high power density, rapid start-up, and immediate response to power changes [5–7]. Compared to SOFCs, MCFCs, and other types of fuel cells that require much higher temperatures of 500–1000 °C [3], PEMFCs usually operate at relatively low temperatures of 100–200 °C. The term 'low temperature' does not appear to be high from an engineering point of view; however, operating PEMFCs at higher temperatures can enhance the effectiveness of PEMs and yield a substantial energy benefits. For example, the adsorption of CO on catalyst

materials decreases with the increase of operating temperature since catalysts are easily poisoned by the adsorbed CO at low operating temperatures [6]. When the operating temperature is higher than 160 °C, CO-induced poisoning of catalysts can be notably suppressed. As a result, PEMFCs can tolerate CO up to 3% and preserve an excellent power performance in hydrogen fuels [8–11]. In addition, high humidity is essential to maintain the proton diffusion in the membranes, but it is not necessary at high temperatures. Low humidity or no humidity can greatly reduce the risk of fuel cell flooding.

In the view of the architecture of a PEMFC, the membrane electrode assembly (MEA) is the most important component, which is a sandwiched three-layer membrane structure comprising of two electrodes, an anode, and a cathode separated by a polymer electrolyte membrane (PEM) (Figure 1). The PEM is at the heart of a PEMFC, as it is crucial to the electrochemical performance of the PEMFC. The roles of the PEM are: (1) to separate the anode and the cathode, (2) to prevent direct contact of the reactant gases (e.g., H₂ and O₂), (3) to allow proton diffusion from the anode to the cathode, (4) to act as an electron nonconductive layer to avoid electrical shortening of the MEA, (5) to force electrons through an external circuit to the cathode, and (6) to provide mechanical integrity to support the electrocatalyst nanoparticles. In addition to the PEM, both the anode and the cathode include Pt nanoparticles as the electrocatalyst.

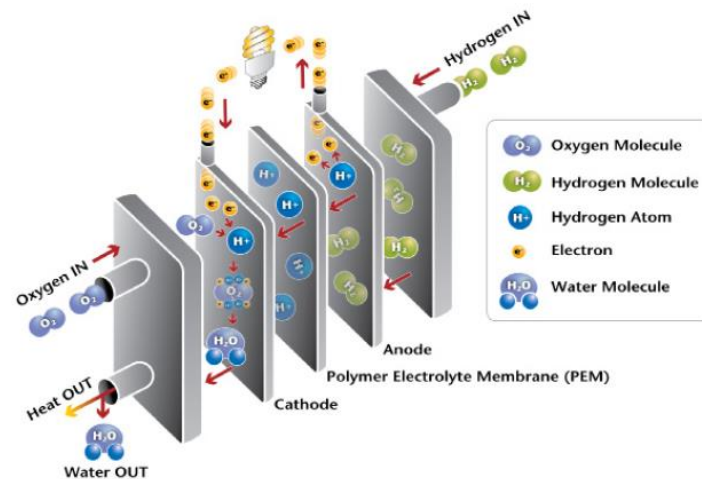
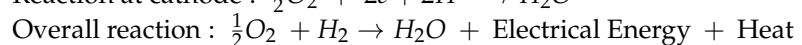
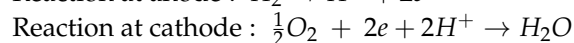


Figure 1. Schematic illustration of a PEMFC, which comprises of an anode and a cathode separated by a PEM (hydrogenandfuelcell.energy.gov).

In a H₂/O₂ PEMFC, as schematized in Figure 1, gaseous hydrogen is fed into the anode and adsorbs onto the catalytic Pt surface, where under Pt electrocatalysis, the hydrogen molecules are split into protons (H⁺) and electrons (e[−]). The protons transport through the PEM in the center toward the other side of the PEMFC, while the electrons transfer through an external circuit to the cathode, thus forming an electrical current that can be used to do work. On the cathode side, the oxygen flows through the channel to the cathode, where it recombines the incoming protons and electrons to form water and potentially useful heat as the only by-products. The anode, cathode, and overall reactions are as follows:



where the produced water can be removed from the fuel cell.

Although varying for different applications, an ideal PEM for PEMFCs must possess the following characteristics, especially for electric vehicle applications:

- (1) High proton conductivity (>0.1 S·cm^{−1}) in a low-humidity environment and at high operation temperatures over 100 °C;

- (2) Low fuel gas permeability;
- (3) Superior electrochemical and thermal stabilities in a harsh environment;
- (4) Excellent mechanical properties in both dry and hydrated states;
- (5) Sufficient water uptake and moderate swelling;
- (6) Outstanding long-term durability (>10 years) in the operating PEMFCs;
- (7) Low cost (<\$10 kW⁻¹ based on a PEMFCs) and easy fabrication.

Since 1970s, DuPont has developed and commercialized the perfluorosulfonic acid (PFSA) ionomer-based membranes, with the commercial trademark Nafion[®], which have been broadly used in PEMFCs because of their extraordinary chemical and thermal stabilities and excellent proton conductivity, $\sim 10^{-1}$ S·cm⁻¹ or higher [6]. The perfluorinated Nafion[®] membranes are composed of carbon–fluorine backbone chains with perfluoro side chains containing sulfonic acid or carboxylic acid groups [7,9]. Their unique chemical structure with functional groups endows them the outstanding hydrophilic property. The unique functional groups also provide Nafion[®] membranes sufficient water uptake, which plays an important role in proton conductivity. Nafion[®] membranes absorb water in amounts dependent upon the number of functional groups. Yet, the dependence of the proton conductivity on the water uptake of Nafion[®] membranes limits the maximum operation temperature, less than 100 °C. A highly hydrated condition is needed to keep the membrane humidification and maintain the proton conductivity, which requires complex cooling and humidifying systems [9,12]. In addition to this drawback, Nafion[®] membranes also have other disadvantages, including their complicated synthesis processes, which leads to high price, \$600–1200 m⁻² [13] and relatively low mechanical and chemical stability at high temperatures [7]. These challenges have driven research to develop low-cost nonfluorinated membrane materials as an alternative to Nafion[®] membranes. Therefore, nonfluorinated membranes with high proton conductivity and high-temperature water-keeping properties are highly desirable to realize their potential as PEMs in high-performance PEMFCs.

Of potential alternatives to Nafion[®] membranes, acid- or alkali-doped polybenzimidazoles (PBIs) are considered as one of the most promising polymeric materials for use as PEMs in PEMFCs [10,14–21]. The acid- or alkali-doped PBI membranes have outstanding properties that allow them to be used as high-temperature PEMs up to 200 °C without dehydration because of the presence of acid or alkaline groups as the proton carriers. Moreover, PBI is a relatively low cost nonperfluorinated polymer and exhibits excellent oxidative and thermal stabilities. Since the ionic conductivity of PBI was first reported over 40 years ago, great efforts have been made to develop PBI membranes for use in fuel cells. Figure 2 shows the annual number of publications for keywords: “polybenzimidazole (PBI)” and “PBI” plus “fuel cell”, respectively, against the calendar year (based on Web of Science). It is notable that in the past two decades, the number of publications on PBI used as PEMs in fuel cells has risen rapidly. Since 2000, the annual number of publications on “PBI + Fuel Cell” has increased more than 16 times. For instance, in 2014 there were 201 and 161 publications for “PBI” and “PBI + Fuel cell,” respectively. Though the annual number of publications slightly decreases after 2014, research in these two fields is still very active, especially in the optimization of PBI membranes and their effects on the performance of PEMFCs.

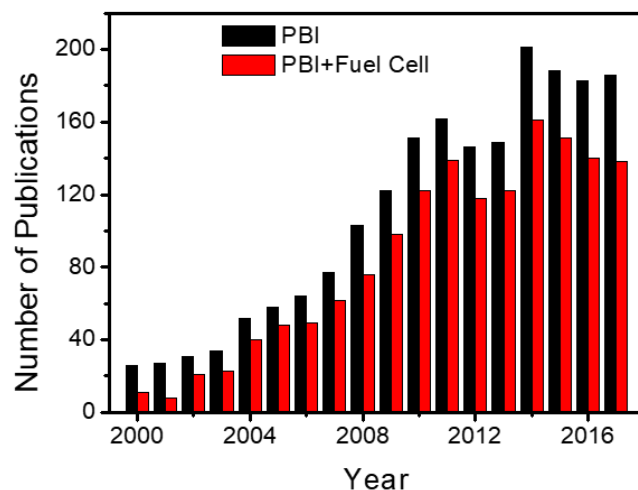


Figure 2. Annual number of publications on “polybenzimidazole” and “fuel cell” since 2000.

Experimental investigations on PBI-based PEMs for use in PEMFCs have been expanded rapidly in recent years. Yet, comprehensive review papers on this subject are still very limited. Thus, in this study we plan to give a timely review on the recent progress in this field. So far, research of PBIs for use as PEMs can be generally classified into three categories: (1) synthesis of broad PBI polymers containing doping groups, (2) acid-doped PBI membranes, and (3) polymeric acid-doped PBI membranes. This review is focused on modification of PBI membranes via various approaches and relevant comparative study of these PBI membranes for PEMFCs. Recently developed novel porous PBI nanofiber membranes for use as PEMs are further reviewed. Conclusions of the present review are made in consequence.

2. Mechanism of Acid Doping for PBI Membranes

Substantial efforts have been made to explore the mechanisms of acid groups interacting with PBI membranes. Kawahara et al. [22] studied the interaction between PBI and strong acids in acid-doped PBI membranes by means of FTIR spectroscopy, and found that acid molecules did not protonate the imidazole groups of PBI. They suggested that acid molecules interacted with hydrogen bonding OH and N groups of the acid-doped PBI membranes. Based on the proton conductivities measured at varying temperatures (30–90 °C) and isostatic pressure (1–4000 bars), Bouchet et al. [23] proposed an activation mechanism. Their experimental observations indicate that the acid anion plays an important role in the proton migration. With this activation mechanism, the isobar and isothermal conductivities determined three characteristic thermodynamic parameters, i.e., the activation volume (ΔV^* , 4–10 cm³/mol), enthalpy (ΔH^* , 0.6–1.1 eV), and entropy (ΔS^* , 40–190 J·mol⁻¹·K⁻¹). The dependences of these three characteristics upon the temperature and pressure were confirmed to be consistent with thermodynamic predictions, and indicated that proton transfers from one imide site to another, in which the anionic species participate.

Ma et al. [24] further confirmed that the proton conductivity of acid-doped PBI membranes strongly depends upon the relative humidity (RH), temperature, and acid-doping level. Accordingly, the temperature dependence of proton conductivity in acid-doped PBI membranes can be explained by the Arrhenius relation:

$$\sigma_T = \sigma_0 \exp(-E_a/RT) \quad (1)$$

where E_a is the activation energy, σ_0 is the pre-exponential factor of proton conductivity, R is the gas constant, and T is the absolute temperature (Kelvin). Given the doping level of an acid-doped PBI membrane, proton conductivity increases with temperature and RH.

With phosphoric acid as a general acid agent for doping PBI membranes, the activation energy decreases with increasing doping level, as a result of excess phosphoric acid in the

acid-doped PBI membranes. Ma et al. [24] observed that the proton migration becomes much easier at a higher acid-doping level, leading to an enhanced proton conductivity at a constant RH and temperature. The increased proton diffusion is expected as a result of excess phosphoric acid in the PBI membranes. As shown in Figure 3b, at lower doping levels of $0 < X < 2$ (X : Phosphoric acid molecules per polymer repeat unit) before the maximum protonation of acid-doped PBI groups is reached, the phosphoric acid anions continuously protonate the N atoms in the imino groups of the doped PBI structure. The formed structure suggests that the proton diffusion mainly occurs between the protonated and nonprotonated imino N groups ($N-H^+ \dots N-H$) on the neighboring polymer chains, leading to relatively low proton conductivity. When the acid-doping level increases above 2, but lower than 3, the protons migrate along the direction of acid-benzimidazole-acid, as shown in Figure 3c. Based on the Grotthuss mechanism [24], the presence of cooperative motion for two protons along the polymer anion chain strongly influences the proton conductivity of acid-doped PBI membranes. As the doping level further increases to $X > 3$, more excess phosphoric acid is doped in the PBI structures, in which the protons mainly migrate along the mixed anionic chains ($H_2PO_4^- \dots H_2PO_4$ and $N-H^+ \dots H_2PO_4^-$), as shown in Figure 3d. In addition, as shown in Figure 3e, the further increased acid level ($4.2 < X < 6$) allows protons to transfer along the acid- H_2O chains or the acid-anion chains ($H_2PO_4^- - H^+ \dots H_2PO_4^-$).

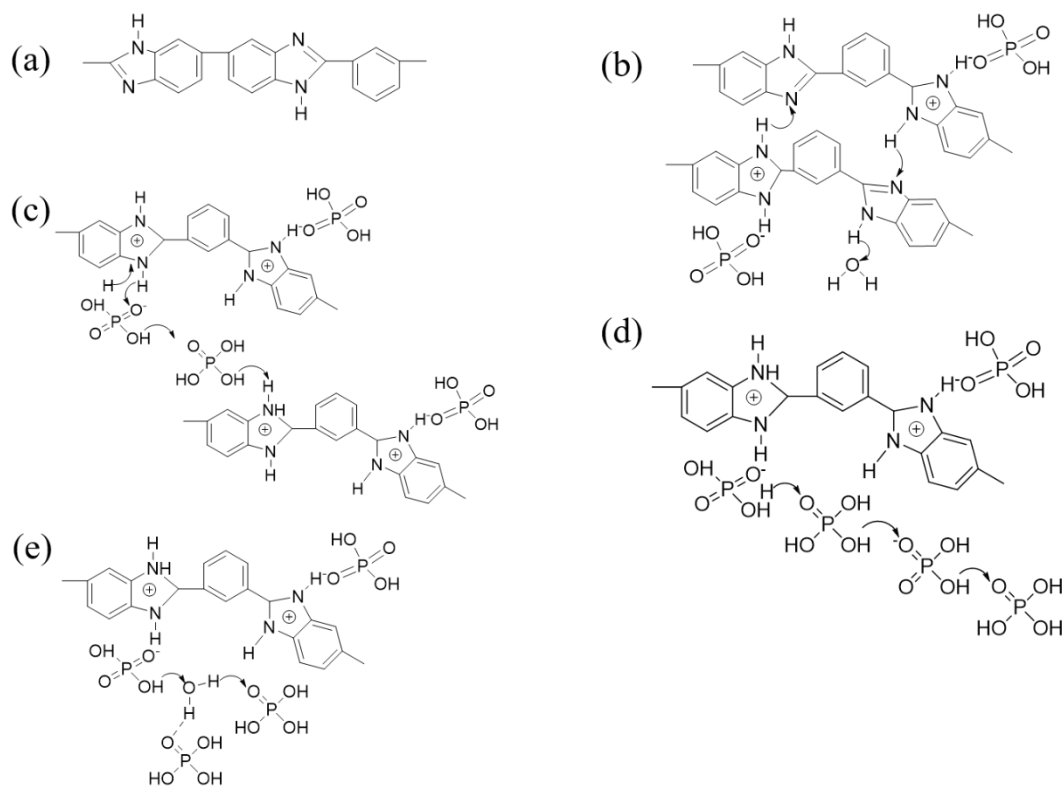


Figure 3. Chemical structures of (a) PBI, (b) phosphoric acid protonated PBI, (c) proton transfers along acid-benzimidazole-acid, (d) proton transfers along acid-acid, and (e) proton transfers along acid- H_2O . Reprint with permission [24]; 2004, The Electrochemical Society.

3. Phosphoric Acid-Doped PBI Membranes for Use as PEMs in Fuel Cells

PBIs carry excellent resistance to inorganic acids and alkalis, even at elevated temperatures. Thus, PBI membranes can almost retain their mechanical and chemical properties after exposure to inorganic acids and alkalis. To improve the proton conductivity of PEMs used in PEMFCs, strong inorganic acids (e.g., H_3PO_4 , H_2SO_4 , $HClO_4$, HNO_3 , and HCl) and inorganic alkalis (e.g., $NaOH$, KOH , and $LiOH$) have been used as doping agents

for various PBIs [25]. These doping agents are compounds with high intrinsic proton conductivity due to their robust hydrogen bond networks and strong, highly polarizable hydrogen bonds [26]. Meanwhile, doped PBI membranes allow the operation of PEMFCs at relatively high temperatures above 100 °C. The complexation of PBI polymers or copolymers containing ether amine or amide groups of strong acidity/basicity can typically form adducts. Recent research has demonstrated that the proton conductivity of acid-doped PBI membranes primarily depends on the types of doping acid agents, the concentration, and other related conditions [25]. The relationship between the proton conductivity of acid-doped PBI membranes and their process parameters raises several outstanding issues, including the choice of acid-doped PBI membranes for the best performance of PEMFCs and mechanisms of acid interactions influencing the proton conductivity in acid-doped PBI systems. To address these issues, the upcoming sections are to review the recent research progress in PBI membranes doped with various types of acids.

Of all the acid agents, phosphoric acid has been most widely used to dope PBI membranes in the last two decades. PBI is a basic polymer that can be easily complexed by a strong acid to form a so-called acid-doped polymer electrolyte. Among others, Wasmus et al. [18] first studied the proton conductivity in phosphoric acid-doped PBI membranes by means of solid-state nuclear magnetic resonance (NMR) and demonstrated that phosphoric acid in PBI membranes has less mobility than that of free phosphoric acid. Wasmus et al. also suggested that interaction exists between PBI structures and phosphoric acid. Such an interaction results in the high proton conductivity and maintains the high thermal stability without external gas humidification. Wainright et al. [27] concluded that direct immersion of PBI membranes into an aqueous solution of phosphoric acid can lead to improved proton conductivity. Utilizing IR spectroscopy, Glipa et al. [28] further confirmed that proton transfers from phosphoric acid to imino groups of PBI as well as the presence of phosphoric acid at a high doping level.

Table 1 summarizes the recent literature works on the physical, chemical, and electrochemical properties of acid-doped PBI membranes for use in fuel cells. According to Wainright's studies [29], the proton conductivity of phosphoric acid-doped PBI membranes depends on the acid-doping level, temperature, and water vapor activity (Figure 4). For example, the proton conductivity of phosphoric acid-doped PBI membranes at the doping level of 501 mole percent (m/o) is two times higher than that of the PBI membranes doped at 338 m/o. In addition to the doping level, proton conductivity also increases with the increase of the treated temperature and water vapor activity. As shown in Figure 4, the highest proton conductivity of $0.04 \text{ S}\cdot\text{cm}^{-1}$ can be achieved at the doping level of 501 m/o, temperature of 190 °C, and water vapor activity of 0.13. To minimize catalyst activity limitation and suppress the poisoning effects from adsorbed intermediates (e.g., CO), PBI membranes need low gas permeability. When used in methanol fuel cells at high temperatures over 200 °C, acid-doped PBI membranes yielded low methanol vapor permeability of $1.5 - 15 \times 10^{-16} \text{ m}^3 \text{ (STP) m/m}^2\cdot\text{s}\cdot\text{Pa}$ and the maximum power density of $0.25 \text{ W}\cdot\text{cm}^{-2}$ at current density of $700 \text{ mA}\cdot\text{cm}^{-2}$. Acid-doped PBI membranes do not require external gas humidification for the operation of fuel cells and maintain the fuel cell performance well without significant decay for over 600 h.

Table 1. Summary of physical, chemical, and electrochemical properties of high-temperature proton exchange PBI membranes for use as PEMs in fuel cells.

Ref. No.	Polymer	Acid/Alkaline Agent	Mechanical Strength (MPa)	Doping Level (wt% or (mol)	Proton Conductivity (σ , S·cm ⁻¹)	Power Density W·cm ⁻²	Ref.
[30]	sulfonated poly [2,2'-(p-oxydiphenylene)-5,5'-bibenzimidazole] (SOPBI)	H ₂ SO ₄	81	154 wt%	1.5×10^{-1} (120 °C)	NA	<i>Polymer</i> 2007 , 48, 5556–5564
[31]	poly(arylene ether sulfone)-b-polybenzimidazole copolymers	H ₃ PO ₄	31	12 mol	4.7×10^{-2} (200 °C)	NA	<i>Polymer</i> 2008 , 49, 5387–5396
[32]	PBz-modified PBI electrospun nanofiber composite	H ₃ PO ₄	115	13.2 mol	1.7×10^{-1} (160 °C)	0.67	<i>J. Mater. Chem. A</i> 2013 , 1, 1171–1178
[33]	sulfonated PBI	H ₂ SO ₄	1.6	~50 mol	3.26×10^{-1} (160 °C)	0.152	<i>Macromolecules</i> 2010 , 43, 6706–6715
[34]	poly(vinylphosphonic acid)-doped PBI (PVPA-PBI)	PVPA	91.1	6.1 wt%	1.72×10^{-2} (120 °C)	0.252	<i>Sci. Rep.</i> 2013 , 3, 1764–1777
[20]	alkaline-doped PBI	KOH	NA	NA	9.5×10^{-2} (25 °C)	0.372	<i>Electrochem. Commun.</i> 2000 , 2, 697–702
[24]	phosphoric acid-doped PBI	H ₃ PO ₄	NA	630 wt%	5.9×10^{-2} (150 °C)	NA	<i>J. Electrochem. Soc.</i> 2004 , 151, A8–A16
[35]	PBI/sulfonated polysulfone (SPSF) polymer blends	polysulfone/ chlorosulfonic acid	NA	5.2 mol	NA	0.54	<i>Electrochem. Solid-State Lett.</i> 2002 , 5, A125–A128
[36]	phosphoric acid-doped PBI	polyphosphoric acid (PPA)	3.5	32 mol	1.0×10^{-2} (RT), 0.26 (200 °C)	0.9	<i>Chem. Mater.</i> 2005 , 17, 5328–5333
[37]	PA-doped PBI composite membranes with ZrP	ZrP/H ₃ PO ₄	NA	5.6 mol	9.0×10^{-2} (200 °C)	NA	<i>J. Membr. Sci.</i> 2003 , 226, 169–184
[38]	PWA/SiO ₂ -doped PBI	phosphotungstic acid (PWA)/SiO ₂	NA	60 wt%	3.0×10^{-3} (100 °C)	NA	<i>J. Power Sources</i> 2000 , 90, 231–235
[39]	SiWA-SiO ₂ -PBI	SiWA-SiO ₂	NA	60 wt%	2.23×10^{-3} (160 °C)	NA	<i>J. Power Sources</i> 2001 , 94, 9–13
[40]	fluorine-containing PBI/HMI-TF composite membranes	1-hexyl-3-methylimidazolium trifluoromethanesulfonate (HMI-TF)	60.3	NA	1.6×10^{-2} (250 °C)	NA	<i>Electrochim. Acta</i> 2011 , 56, 2842–2846
[41]	SrCeO ₃ -PBI composite membrane	strontium cerate (SrCeO ₃)	NA	190 wt%	1.05×10^{-1} (180 °C)	0.44	<i>Electrochim. Acta</i> 2015 , 154, 370–378
[42]	PBI/DAlm TIPN membrane	poly(1, 2-dimethyl-3-allylimidazolium) (PDAlm)/KOH	48.2	2.89 wt%	9.67×10^{-2} (80 °C)	NA	<i>Electrochim. Acta</i> 2017 , 257, 9–19
[43]	sulfonated PES/PBI blend membrane	sulfonated poly(ether sulfone) (PES)/PPA	NA	98 wt%	1.21×10^{-1} (70 °C)	0.11	<i>Eur. Polym. J.</i> 2010 , 46, 1633–1641

Table 1. Cont.

Ref. No.	Polymer	Acid/Alkaline Agent	Mechanical Strength (MPa)	Doping Level (wt% or (mol)	Proton Conductivity (σ , S·cm ⁻¹)	Power Density W·cm ⁻²	Ref.
[44]	PBI/KOH membrane	KOH	7.7	NA	1.84×10^{-2} (RT)	0.031	<i>Int. J. Hydrogen Energy</i> 2008 , 33, 7172–7176
[45]	PA/PBI membrane	H ₃ PO ₄	NA	45 wt%	NA	0.12	<i>Int. J. Hydrogen Energy</i> 2009 , 34, 9479–9485
[46]	CeSPP-doped PBI composite membrane	Cerium sulfophenyl phosphate (CeSPP)	18	NA	1.1×10^{-1} (100% RH), 2.4×10^{-3} (0% RH), (180 °C)	NA	<i>Int. J. Hydrogen Energy</i> 2017 , 42, 486–495
[47]	PA-doped PBI/graphene oxide composite membrane	H ₃ PO ₄	NA	13 wt%	1.704×10^{-1} (165 °C)	0.38	<i>Int. J. Hydrogen Energy</i> 2017 , 42, 2636–2647
[48]	PA-doped PBI/ZrP composite membrane	H ₃ PO ₄	119	15.4 wt%	2.0×10^{-1} (180 °C)	NA	<i>Int. J. Hydrogen Energy</i> 2017 , 42, 2648–2657
[49]	PA-doped PBI membrane	H ₃ PO ₄	NA	75 wt%	6.2×10^{-2} (150 °C, 30% RH)	0.185	<i>J. Electrochem. Soc.</i> 2004 , 151, A304–A310
[50]	crosslinked PBI-TEBP membrane	H ₃ PO ₄	77.11	7.9 mol	5.1×10^{-2} (150 °C)	NA	<i>J. Mater. Chem.</i> 2011 , 21, 2187–2193
[51]	PBI-TGIC/SPANi composite membrane	triglycidylisocyanurate (TGIC)/sulfonated polyaniline (SPANi)/H ₂ SO ₄	21	NA	1.3×10^{-1} (180 °C, 100% RH); 1.8×10^{-2} (180 °C, 0% RH)	NA	<i>J. Membr. Sci.</i> 2018 , 549, 660–669
[52]	crosslinked metal oxide containing PBI composite membrane	sulfonated TiO ₂ particles/H ₃ PO ₄	8	392 wt%	9.8×10^{-2} (160 °C)	0.356	<i>J. Membr. Sci.</i> 2018 , 560, 11–20
[53]	side-chain PBI membrane	PPA	34.3	12.15 wt%	1.1×10^{-1} (80 °C)	NA	<i>J. Membr. Sci.</i> 2018 , 546, 15–21
[54]	PA-doped crosslinked PBI-OO membranes	H ₃ PO ₄	11	266 wt%	2.6×10^{-1} (160 °C)	0.452	<i>J. Membr. Sci.</i> 2017 , 544, 416–424
[55]	pyridine-containing PBI membrane	H ₃ PO ₄	12.3	250 wt%	8.3×10^{-2} (160 °C), 1.1×10^{-2} (25 °C)	0.460	<i>J. Membr. Sci.</i> 2016 , 502, 29–36
[56]	PBI containing bulky substituents	tetraamines and 4,4'-oxybis (benzoic acid)	8.7	245 wt%	8.8×10^{-2} (160 °C)	0.636	<i>J. Membr. Sci.</i> 2016 , 513, 270–279
[57]	PA-doped PBI/PBI-EPA blend membrane	H ₃ PO ₄	59.4	260 wt%	6.8×10^{-2} (160 °C)	0.527	<i>J. Membr. Sci.</i> 2015 , 491, 10–21
[58]	hydroxyl pyridine containing PBI membrane	H ₃ PO ₄	4.6	72 wt%	1.02×10^{-1} (180 °C)	0.57	<i>J. Membr. Sci.</i> 2013 , 446, 318–325
[59]	PBI-functionalized SiO ₂ composite membrane	H ₃ PO ₄	98	385 wt%	5.0×10^{-2} (160 °C)	0.65	<i>J. Membr. Sci.</i> 2012 , 403–404, 1–7

Table 1. Cont.

Ref. No.	Polymer	Acid/Alkaline Agent	Mechanical Strength (MPa)	Doping Level (wt% or (mol)	Proton Conductivity (σ , S·cm ⁻¹)	Power Density W·cm ⁻²	Ref.
[60]	PBI/1H-imidazole-4-sulfonic acid hybrid membrane	1H-imidazole-4-sulfonic acid	33.8	8 mol	7.0×10^{-2} (160 °C)	NA	<i>J. Membr. Sci.</i> 2012 , 399–400, 11–15
[61]	PBI-clay composite membrane	H ₃ PO ₄	105	12 mol	1.2×10^{-1} (150 °C)	0.23	<i>J. Membr. Sci.</i> 2011 , 383, 78–87
[62]	PA-doped PBI membrane	PPA	176	17.2 mol	5.3×10^{-2} (180 °C)	NA	<i>J. Membr. Sci.</i> 2010 , 347, 69–74
[63]	crosslinked PBI containing branching structure	H ₃ PO ₄	78.4 (undoped), 16.9 (doped)	197.1 wt%	3.8×10^{-2} (180 °C)	0.404	<i>J. Power Sources</i> 2018 , 389, 222–229
[64]	dimensionally stable PA-doped PBI membrane	PPMA	111.5 (undoped); 10 (doped)	24.6 mol	2.17×10^{-1} (200 °C)	0.32	<i>J. Power Sources</i> 2016 , 336, 391–400
[65]	Poly (2, 5-benzimidazole) (AB-PBI) membrane	H ₃ PO ₄	NA	6 mol	NA	0.305	<i>J. Power Sources</i> 2014 , 270, 627–633
[66]	phenylindane-containing PBI membrane	PPA	76 (undoped), 10 (doped)	10 mol	6.1×10^{-2} (180 °C)	0.36	<i>J. Power Sources</i> 2013 , 243, 796–804
[67]	ionic liquid doped PBI membrane	1-H-3-methylimidazolium bis (trifluoromethane-sulfonyl) imide	NA	NA	1.86×10^{-3} (190 °C)	0.039	<i>J. Power Sources</i> 2013 , 222, 202–209
[27]	PVA-PBI polymer blend membrane	KOH	40	35 wt%	1.03×10^{-1} (90 °C)	0.076	<i>Renewable Energy</i> 2018 , 127, 883–895
[68]	polybenzimidazolium halides	isophthalic acid/a,a'-dibromo-p-xylene	NA	NA	5.8×10^{-2} (60 °C), 2.9×10^{-2} (26 °C)	0.015	<i>Macromol. Mater. Eng.</i> 2011 , 296, 899–908
[29]	phosphoric acid-doped PBI	H ₃ PO ₄	NA	5 mol	2.0×10^{-2} (150 °C)	0.25	<i>J. Electrochem. Soc.</i> 1995 , 142, 121–123
[69]	alkali doped PBI membrane	KOH	NA	NA	1.84×10^{-2} (25 °C)	0.061	<i>J. Power Sources</i> 2008 , 182, 95–99
[70]	alkali doped PBI membrane	KOH	NA	NA	4.92×10^{-2} (90 °C)	0.112	<i>Int. J. Hydrogen Energy</i> 2013 , 38, 10602–10606
[71]	alkali doped PBI membrane	KOH	NA	NA	2.3×10^{-2} (60 °C)	0.016	<i>J. Power Sources</i> 2011 , 196, 3244–3248
[72]	sulfonated PBI membranes	H ₂ SO ₄	1198	NA	8×10^{-2} (120 °C)	NA	<i>J. Membr. Sci.</i> 2008 , 314, 247–256
[73]	sulfonated thermal treatment PBI membranes	H ₂ SO ₄	NA	NA	2.4×10^{-5} (20 °C)	NA	<i>Desalination</i> 2002 , 147, 183–189
[74]	sulfonated PBI membranes	H ₂ SO ₄	NA	NA	7.5×10^{-5} (160 °C)	NA	<i>J. Membr. Sci.</i> 2001 , 188, 71–78

Table 1. Cont.

Ref. No.	Polymer	Acid/Alkaline Agent	Mechanical Strength (MPa)	Doping Level (wt% or (mol)	Proton Conductivity (σ , S·cm ⁻¹)	Power Density W·cm ⁻²	Ref.
[75]	sulfuric and phosphoric acid doped PBI	H ₂ SO ₄ /H ₃ PO ₄	NA	NA	4×10^{-3}	NA	<i>J. Mater. Chem.</i> 1999 , <i>9</i> , 3045–3049
[76]	sulfonated ABPBI with phosphoric acid	H ₂ SO ₄	NA	49 wt%	3.5×10^{-2} (185 °C)	NA	<i>Electrochim. Acta.</i> 2004 , <i>49</i> , 4461–4466
[28]	sulfonated PBI membranes compared to Nafion	H ₂ SO ₄	NA	75 wt%	5.4×10^{-2}	NA	<i>Solid State Ionics</i> 1997 , <i>97</i> , 323–331

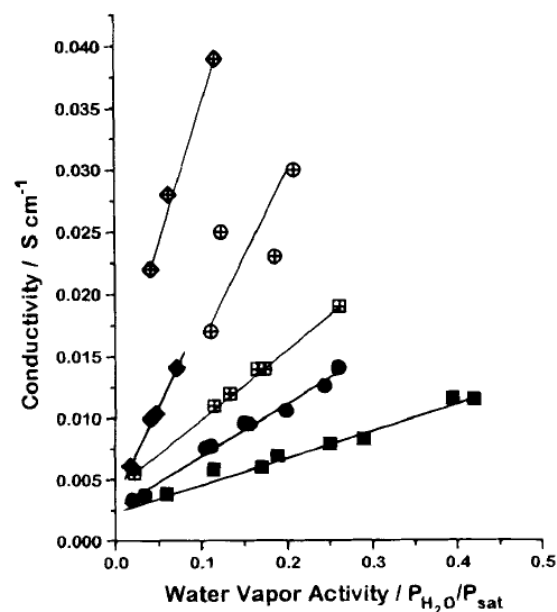


Figure 4. Proton conductivity of phosphoric acid-doped PBI membranes as a function of acid-doping level, temperature, and water vapor activity (partial pressure of water is normalized to the saturated vapor pressure). Filled and open symbols are referred to doping levels of 338 and 501 m/o, respectively. 130 °C (■,▣), 150 °C (●,⊕), 190 °C (◆,◇). Reprint with permission [29]; 1995, The Electrochemical Society.

In high-temperature PEMFCs, high concentration of phosphoric acid is required to provide the high proton mobility within the PEMs. As the phosphoric acid-doping level increases, large amount of liquid phosphoric acid on the electrolyte–electrode interface and within the electrodes delays or even blocks gas transport and impedes the electrode reactions by phosphate anion adsorption on Pt catalyst layers. Such situation raises two outstanding issues. The first is how the distribution of phosphoric acid influences the performance of PEMFCs; the second is how to optimize the assemblies of the PEMs and electrodes [45]. Hence, new strategies to design MEAs are highly desirable. Conventionally, phosphoric acid-free approaches were required to assemble highly acid-doped membranes and gas diffusion electrodes. Alternative strategies were reported to combine dried membranes or catalyst-coated membranes with phosphoric acid-complexed gas diffusion electrodes in order to simplify the MEAs in PEMFCs [15,77]. To elucidate the optimal phosphoric acid impregnation strategies and the effect of phosphoric acid on the performance of PEMFCs, Wannek et al. [45] conducted comprehensive studies on high-temperature PEMFCs assembled by phosphoric acid-doped PBI membranes. Their study indicated that redistribution of phosphoric acid in PEMFCs is a rather quick process, implying that at the beginning few minutes of cell operation, the amount of phosphoric acid

transferred to the PBI membrane is high and results in the high initial proton conductivity. A dynamic equilibrium of phosphoric acid distribution is established after a few hours. As a result, the distribution of phosphoric acid in the steady state and the fuel cell performance were found to be independent of the way to introducing phosphoric acid into the PBI membranes.

In addition to phosphoric acid-doped PBI membranes, Asensio et al. [49] reported that poly(2,5-benzimidazole)(AB-PBI) membranes could be prepared by casting methanesulfonic acid (MSA) and then impregnated in a phosphoric acid bath for 3 days. To obtain a similar acid doping level of 75 wt%, AB-PBI membranes need the phosphoric acid concentration lower than that of poly [2,2'-(*m*-phenylene)-5,5' bibenzimidazol] (*m*-PBI). It took only a few minutes for AB-PBI membranes to absorb nearly all of the allowable phosphoric acid. To remove the water absorbed from the acid solutions, the acid-doped AB-PBI membranes were dried at 100 °C. As shown in Figure 5, the highest proton conductivity for acid-doped AB-PBI membranes was 0.062 S·cm⁻¹ at 150 °C and 30% RH. The proton conductivity was found to increase with increasing either temperature or RH. The authors also found both acid-doped AB-PBI and *m*-PBI membranes to carry the similar proton conductivity and performance in the fabricated PEMFCs, leading to a preferable alternative to PBI.

Inorganic nanomaterials (e.g., carbon nanotubes (CNTs), graphene oxides, silica nanoparticles, and clay nanoparticles) into PBI membranes were reported to improve the acid-doping level and proton conductivity of PBI membranes [12,47,61,78]. The incorporated inorganic nanomaterials also influence the mechanical and thermal properties of the resulting PBI membranes [79]. Üregen et al. [47] prepared phosphoric acid-doped PBI/graphene-oxide nanocomposite membranes for use in PEMFCs. Figure 6 shows the graphene oxides dispersed uniformly in the PBI polymer matrix. The even distribution can be attributed to the rich oxygen-containing functional groups, which can facilitate the interfacial regions with the PBI via covalent or noncovalent structures [80,81]. With the addition of graphene oxides at 2 wt% and an acid-doping level of 13, the PBI membranes exhibited the highest proton conductivity of 0.1704 S·cm⁻¹, resulting in the high power density of 0.38 W·cm⁻². The high proton conductivity and resulting superior fuel cell performance can be attributed to the chemical interactions between PBI and graphene oxides and the rich oxygen-containing functional groups of graphene oxides.

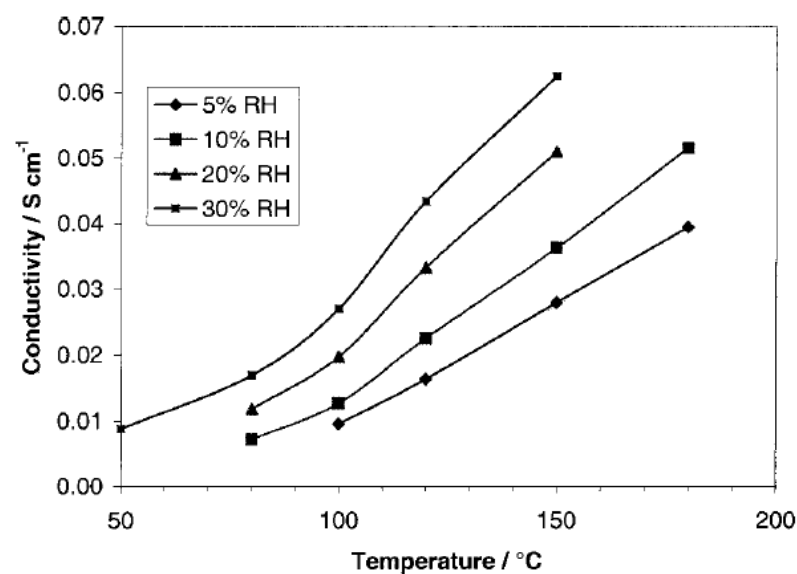


Figure 5. Typical scanning electron microscopy (SEM) micrographs of (a) top surface of a pure PBI membrane and (b–d) cross sections of PBI/graphene-oxide nanocomposite membranes at varying magnifications from low to high. Reprint with permission [47]; 2004, Elsevier.

Sulfonated graphene oxides have been used to enhance the proton conductivity of PBI membranes and PEMFC performance [82]. Similar to the PBI/graphene oxides, the PBI/sulfonated graphene oxides have homogeneous structures through the cross section of the membrane (Figure 7A,B). Doped only with low phosphoric acid content, the PBI/sulfonated graphene oxides exhibited high proton conductivity of $0.052 \text{ S}\cdot\text{cm}^{-1}$ at $175 \text{ }^\circ\text{C}$, two times higher than that of PBI/graphene oxides and PBI membranes. These results suggest that a low phosphoric acid-doping level reduced the free acid in the PBI membranes, which avoided water loss and proton conductivity loss. Because of the high proton conductivity, the PBI/sulfonated graphene-oxide nanocomposite membranes in the PEMFCs produced a peak power density of $600 \text{ mW}\cdot\text{cm}^{-2}$ at $175 \text{ }^\circ\text{C}$ and H_2/O_2 atmospheric pressure (Figure 7C).

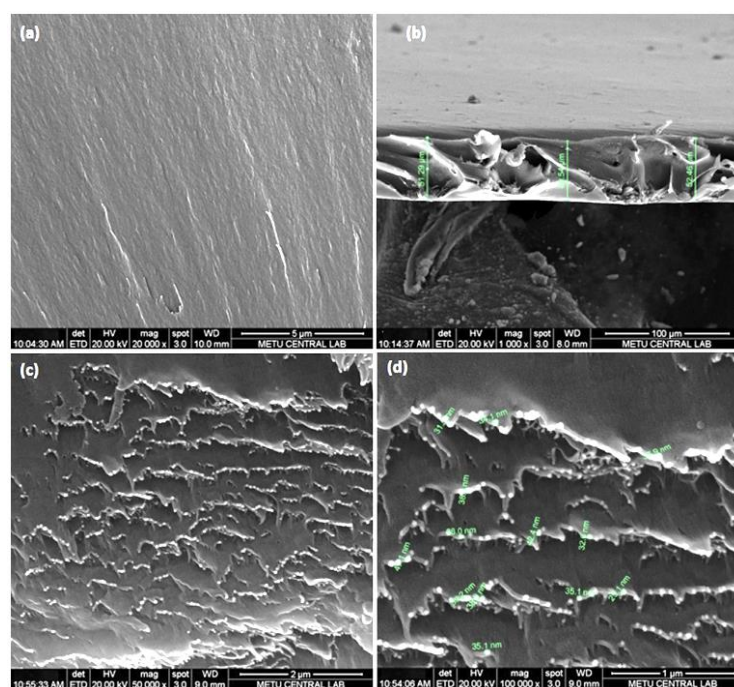


Figure 6. SEM micrographs of the cross section of (A) PBI/graphene oxides and (B) PBI/sulfonated graphene-oxide nanocomposite membranes after phosphoric acid-doping; (C) polarization and power density curves of a PEMFC operated at $175 \text{ }^\circ\text{C}$ and H_2/O_2 atmospheric pressure. Reprinted with permission [82], 2011, Royal Society of Chemistry.

As demands on PEMFCs are increasing, an ideal electrolyte polymer membrane requires not only high proton conductivity, but also durable mechanical properties [61,83]. To meet the demands of PEMFCs, Plackett et al. [61] fabricated homogeneous and transparent PBI/laponite clay nanocomposite membranes. With addition of modified laponite clay nanoparticles into PBI, the resulting nanocomposite membranes were then directly placed in an 80–85 wt% phosphoric acid solution at $50 \text{ }^\circ\text{C}$ for 20 h. As a result, the acid-doped PBI/clay nanocomposite membranes carried the high acid-doping levels of >8 , indicating the excess of phosphoric acid in the nanocomposite membranes. The excess of phosphoric acid and the incorporated clay nanoparticles in the PBI membranes led to the high proton conductivity of $0.12 \text{ S}/\text{cm}$ at the acid-doping level of 12, temperature of $150 \text{ }^\circ\text{C}$, and 12% RH. In addition, without phosphoric acid doping, all PBI/clay nanocomposite membranes containing respectively 10 wt%, 15 wt%, and 20 wt% of clay nanoparticles exhibited high tensile strength in the range of 90 to 120 MPa and elongation of 3% to 5%. After phosphoric acid doping, the tensile strength of the PBI/clay nanocomposite membranes significantly decreased to the range of 4 to 8 MPa, but the elongation at break increased up to 231.8% at $150 \text{ }^\circ\text{C}$ and ambient humidity. Another advantage of the use of laponite clay nanoparticles for composite membranes is their low hydrogen

permeability. Compared to the pristine PBI membranes, the PBI/clay nanocomposite membranes possessed much lower hydrogen permeability ranging from 0.6×10^{-10} to $1.2 \times 10^{-10} \text{ mol}\cdot\text{cm}^{-1}\cdot\text{s}^{-1}\cdot\text{bar}^{-1}$.

To improve the high-temperature performance of PEMFCs, Özdemir et al. [48] prepared PBI based nanocomposite membranes incorporated with inorganic fillers as the conductive material additive. The proton conductivities of the nanocomposites based on three types of inorganic nanoparticle fillers—i.e., TiO_2 , SiO_2 , and ZrP—were compared. The compatibility of these fillers with PBI matrix plays an important role in the mechanical and thermal properties as well as the proton conductivity of the resulting nanocomposite membranes. As shown in Figure 8, SiO_2 nanoparticles were well-dispersed in the PBI matrix to form a relatively homogeneous structure. Yet, both ZrP and TiO_2 nanoparticles were observed on the cross-section areas, indicating nonhomogeneous structures formed in the PBI matrix, especially for TiO_2 nanoparticles with clear sedimentation. Compared to the pristine PBI membranes, the tensile strength and elongation of PBI based nanocomposite membranes reinforced with 5 wt% ZrP nanoparticles only decreased slightly. In addition, the PBI/ TiO_2 nanocomposite membranes exhibited the lowest tensile strength of 85.6 MPa and the lowest elongation of 34% due to the nonhomogeneous distribution of the TiO_2 nanoparticles in PBI matrix. These PBI nanocomposite membranes were immersed directly in 85 wt% phosphoric acid solution for 264 h. The PBI/ZrP nanocomposite membranes after acid treatment exhibited a high acid-doping level of 15.4, leading to the highest proton conductivity of $0.2 \text{ S}\cdot\text{cm}^{-1}$ at 180°C (Figure 8). The proton conductivity of the PBI/ZrP nanocomposite membranes is much higher than that of all other membranes in the temperature range of $140\text{--}180^\circ\text{C}$ as the result of different interactions between PBI and these conductive nanoparticle fillers.

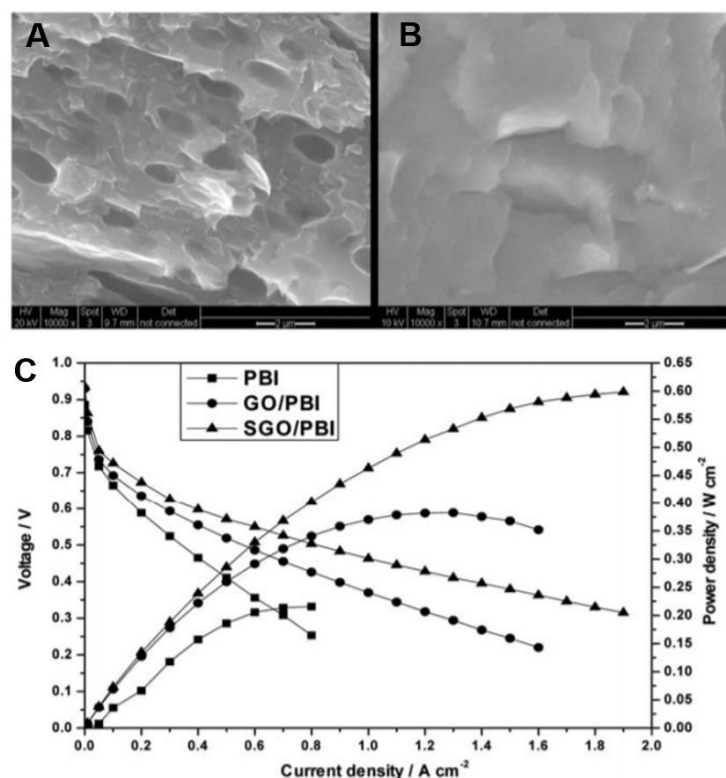


Figure 7. Variation of the proton conductivity of phosphoric acid-doped AB-PBI membranes with varying temperatures ($50\text{--}180^\circ\text{C}$) at four different RHs. Reprint with permission [49]; 2004, The Electrochemical Society.

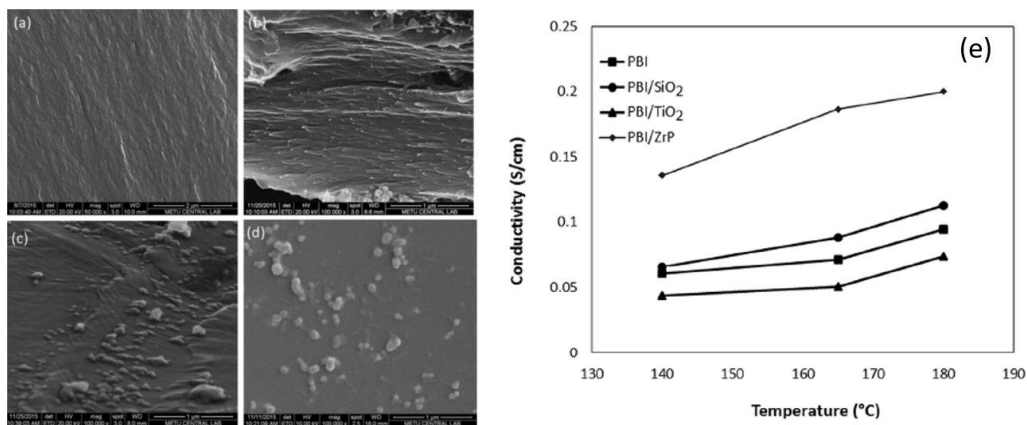


Figure 8. SEM micrographs of (a) PBI membrane, (b) PBI/SiO₂ nanocomposite membrane, (c) PBI/ZrP nanocomposite membrane, (d) PBI/TiO₂ nanocomposite membrane, and (e) proton conductivities of PBI and PBI nanocomposite membranes. Reprinted with permission [48], 2007, Elsevier.

Mack et al. [65] studied the effects of doping time and temperature on the proton conductivity of phosphoric acid-doped PBI membranes and their fuel cell performance. They found that the doping level of PBI membranes increased with doping time at all given temperatures (Figure 9A). Both doping time and temperature played important roles in the proton conductivity of doped PBI membranes (Figure 9B). Short acid-doping times results in low doping level and nonuniform acid distribution across the PBI membranes, which leads to the low fuel cell performance (Figure 9C). As the acid-doping level increases, the amount of phosphoric acid increases from the surface to the middle of the PBI membranes and more imidazole groups of PBI in the center of the membranes are contacted with the phosphoric acid. Mack et al. [65] suggested that a sufficient amount of phosphoric acid could be optimized by controlling the acid-doping time and temperature (Figure 9D). In addition to the acid-doping level, acid distribution inside the PBI membranes is also crucial in order to achieve the high proton conductivity and fuel cell performance.

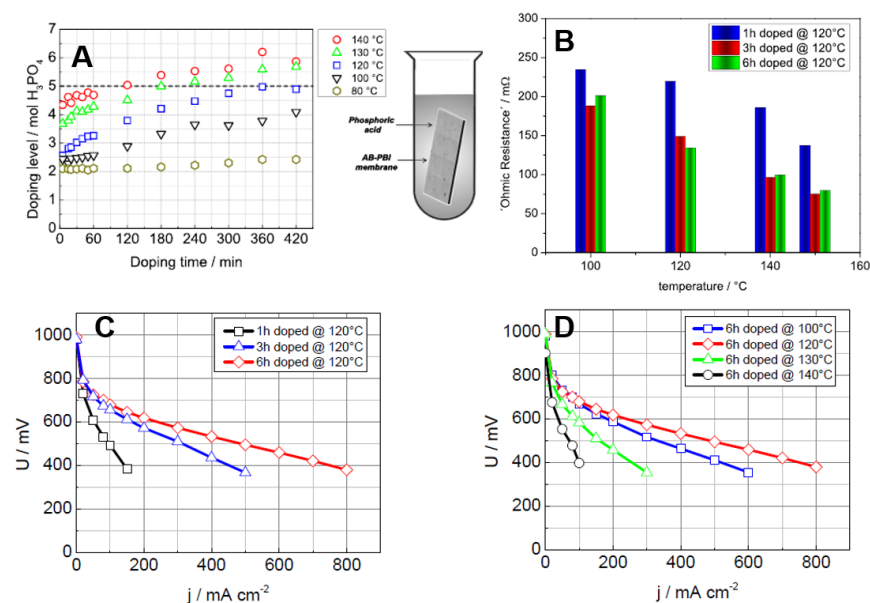


Figure 9. (A) Scheme of an AB-PBI membrane immersed in phosphoric acid (right) and the increase of acid-doping level of AB-PBI membranes with doping time; (B) ex situ proton conductivity of AB-PBI membranes after acid doping for 1, 3, and 6 h, respectively; (C) cell performance depending on doping time of AB-PBI membranes doped at 120 °C; (D) cell performance depending on doping temperature of AB-PBI membranes doped for 6 h. Reprinted with permission [65], 2014, Elsevier.

4. Sulfuric Acid-Doped and Sulfonated PBI Membranes for Fuel Cells

In addition to phosphoric acid-doped PBI membranes, sulfuric acid-doped and sulfonated PBI membranes have been developed recently because of their high proton conductivities, which are less dependent on doping level. Glipta et al. [75] have reported that sulfuric acid can be loaded in PBI membranes to form a PBI-sulfuric acid complex membrane (Figure 10).

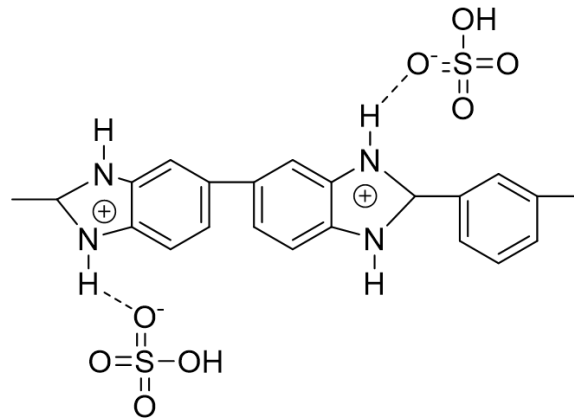


Figure 10. Schematic configuration of sulfuric acid-protonated PBI structures.

There are three primary ways to synthesize sulfonated PBI. The first is to chemically modify the PBI backbone using sulfonating reagents (e.g., 4-bromomethylbenzene sulfonic acid sodium salt and alkanesultone) [28,84]. The second is to directly polymerize sulfonated PBI with the sulfonated dicarboxylic acid monomers [49,74]. Although desired sulfonated PBI structures and control of the degree of sulfonation can be achieved through this method, it is difficult to synthesize the sulfonated monomers because most of the sulfonated monomers are not commercially available. The third is post-sulfonation of PBI through thermal annealing of sulfuric acid-doped PBI membranes at a high temperature (450–475 °C) [85]. The post-sulfonation approach is quite simple, but it usually reduces the mechanical properties of the resulting membranes and only a low degree of sulfonation can be achieved after high-temperature treatment.

Recently, Xu et al. [30] reported the synthesis of sulfonated poly [2,2'-(p-xylylene)-5,5'-bibenzimidazole] (SOPBI) through post-sulfonating reaction with a synthesized OPBI polymer (Figure 11). Compared to direct polymerization, post-sulfonation of PBI is very useful and facile process for preparing SOPBI with controllable degree of sulfonation. The post-sulfonation process was conducted with sulfuric acid as the sulfonating reagent at 80 °C. After post-sulfonation, SOPBI showed no significant degradation and a good solubility in DMSO, and it maintained high thermal stability and excellent mechanical properties. SOPBI also possessed the high proton conductivity of 0.15 S·cm⁻¹ at 120 °C in water as well as good water stability and radical oxidative stability. In addition, the proton conductivity of sulfonated PBI membranes relied strongly on the degree of sulfonation, which increased with increasing degree of sulfonation.

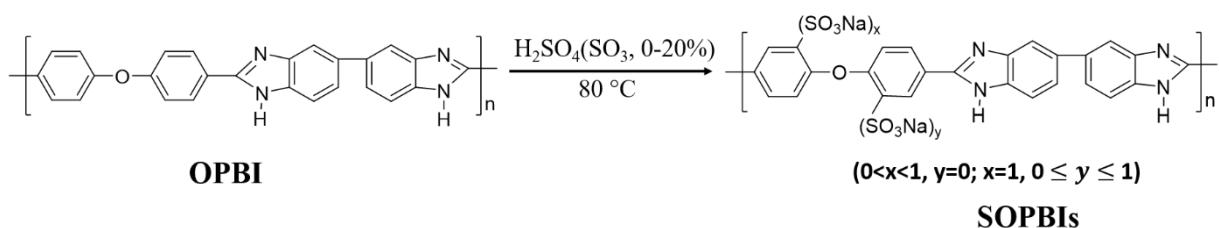


Figure 11. Post-sulfonation of poly [2,2'-(p-xylylene)-5,5'-bibenzimidazole] (OPBI) membranes. Reprinted with permission of [30], 2007, Elsevier.

Similar to phosphoric acid-doped PBI membranes, the sulfuric acid-loaded level in PBI membranes is crucial to the proton conductivity and fuel cell performance. Studies by Savadogo et al. [21] demonstrated that the proton conductivity of sulfuric acid-doped PBI membranes was higher than that of phosphoric acid-doped PBI membranes. Under non-humidified hydrogen/oxygen conditions, MEAs based on sulfuric acid-doped PBI membranes exhibited a higher proton conductivity and thus higher fuel cell performance than those based on Nafion® membranes. In addition, as reported by Glipa et al. [28], after immersed in a sulfuric acid solution for 2–3 h, sulfuric acid-doped PBI membranes possessed a high proton conductivity comparable to that of phosphoric acid-doped PBI membranes.

Wu and Scott [86] investigated the interplay among sulfuric acid-doping level, immersion time, sulfuric acid concentration, and the operating temperature on the proton conductivity of sulfuric acid-doped PBI membranes and fuel cell performance. In general, the sulfuric acid-doping level in PBI membranes increased with increasing concentration of sulfuric acid solutions and immersion time (Figure 12A). As shown in Figure 12B, proton conductivity increases dramatically from about 0.02 to 0.112 S·cm⁻¹ as the RH increases from 9.7% to 38% at a given acid-doping level of 3.17. Enhanced proton conductivity corresponds to improved fuel cell performance (Figure 12C,D). Yet, the maximum power density decreases from 137 to 71 mW·cm⁻² as the operating temperature increases from 80 to 120 °C. This phenomenon is different from phosphoric acid-doped PBI membranes, based on which the fuel cell performance increases with the operating temperature. This could be explained by considering the resistance of the sulfuric acid-doped PBI membranes, which increases in the catalyst layers with increasing temperature.

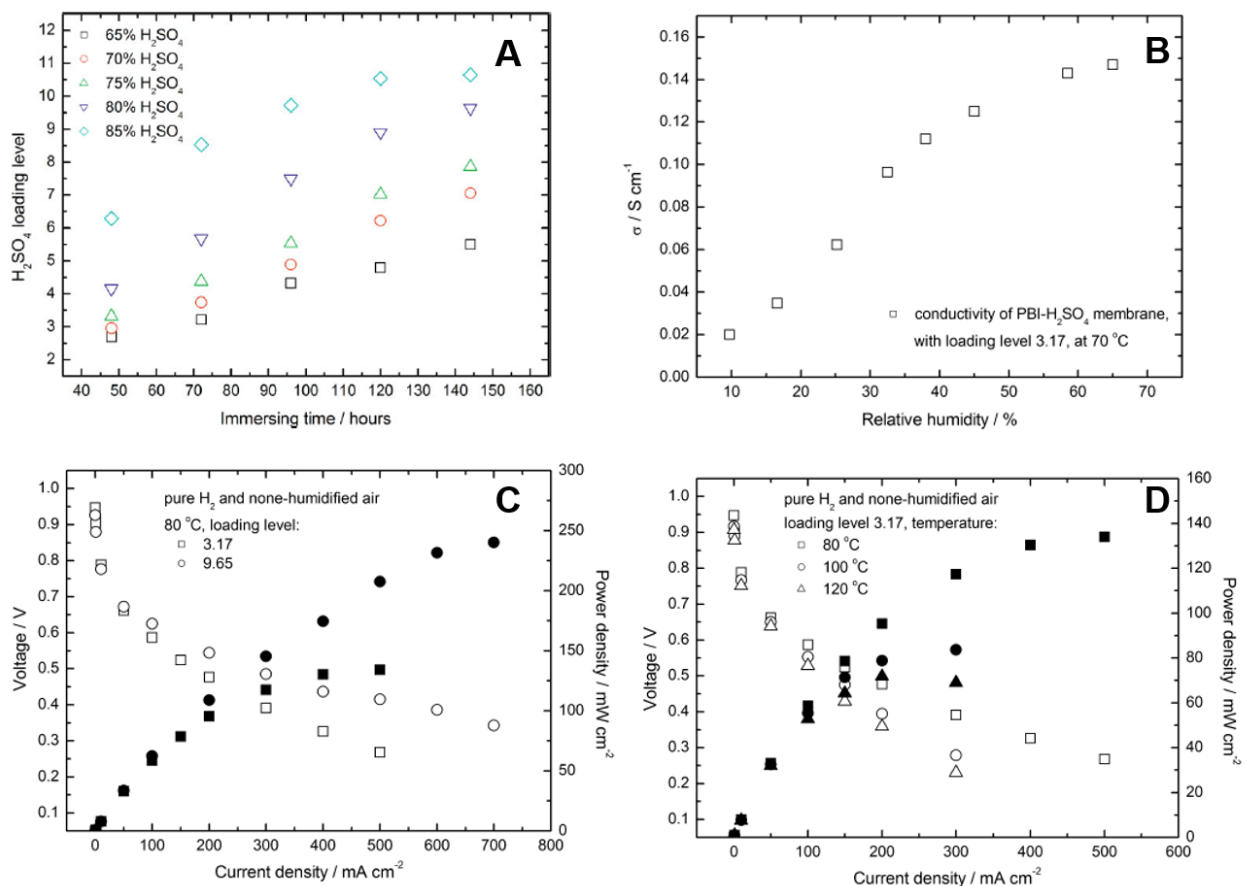


Figure 12. (A) Dependence of the sulfuric acid-doping level of PBI membranes upon the immersion time and sulfuric acid concentration; (B) dependence of the sulfuric acid-doped PBI membranes upon RH; (C) the polarization and power density curves of fuel cells based on sulfuric acid-doped PBI membranes; (D) influence of the operating temperature on the fuel cell performance based on sulfuric acid-doped PBI membranes. Reprinted with permission [86], 2004, Wiley-VCH.

It has been reported that phosphoric acid-doped sulfonated PBI membranes possessed higher proton conductivity than the counterpart phosphoric acid-doped PBI membranes. Mader and Benicewicz [33] synthesized the high-molecular-weight, highly phosphoric acid-doped sulfonated PBI membranes using polycondensation of a sulfonated aromatic diacid with an aromatic tetraamine (Figure 13). Advantages of this approach include limitation of side reactions and control over the degree of sulfonation. Phosphoric acid-doped sulfonated PBI membranes exhibited excellent proton conductivities up to $0.326 \text{ S}\cdot\text{cm}^{-1}$ when the temperature increased to $180 \text{ }^\circ\text{C}$. The proton conductivity increased with the acid-doping level but did not show any further increase at the acid-doping levels higher than 39 mol phosphoric acid/PBI. This is due likely to the failure of the acid-doped PBI membranes to hold a large amount of acid molecules and still maintain the mechanical strength. These membranes possessed the high acid loadings of $>30 \text{ mol}$ phosphoric acid/PBI. More importantly, the fuel cells with the sulfonated PBI membranes had excellent performance with the maximum voltage of 0.76 V at $0.2 \text{ A}\cdot\text{cm}^{-2}$ and $160 \text{ }^\circ\text{C}$ (Figure 14).

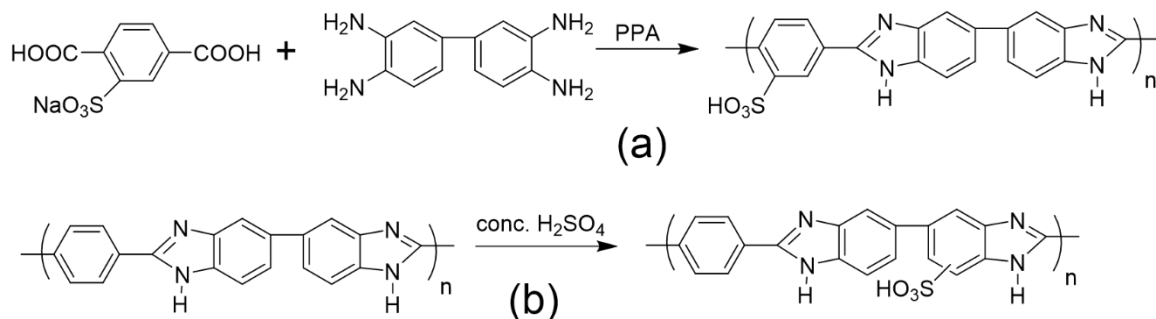


Figure 13. (a) Direct polymerization of *s*-PBI from a sulfonated diacid and tetraamine and (b) post-sulfonation of *p*-PBI to produce *s*-PBI. Reprinted with permission [33], 2010, the American Chemical Society.

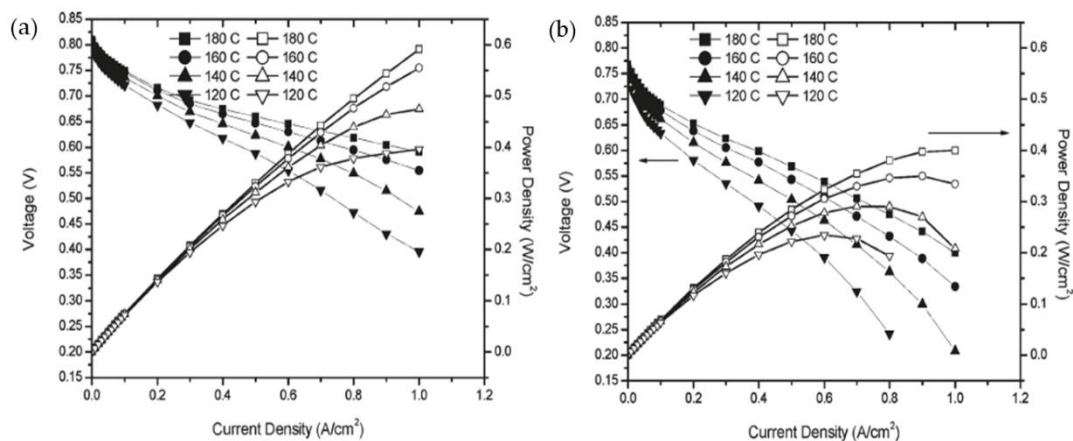


Figure 14. Fuel cell performance of phosphoric acid-doped sulfonated PBI membranes: Polarization curves (filled symbols) and power density curves (open symbols) with (a) hydrogen/oxygen and (b) hydrogen/air. Reprinted with permission [33], 2010, the American Chemical Society.

5. Polymeric Acid-Doped PBI Membranes

Inorganic acid-doped PBI membranes have been extensively investigated as promising alternatives to high-temperature PEMs for PEMFCs. Yet, PBI membranes after acid treatment typically suffered from their poor mechanical properties. Highly phosphoric acid-doped PBI membranes require complex post-processes prior to use in fuel cells. To retain the original mechanical properties of the pristine PBI membranes and eliminate the com-

plex post-processes, polymeric acids have been widely used as an efficient condensation agent for synthesis of high-temperature fuel cell PBI membranes [87].

Makoto et al. [88] demonstrated that polyphosphoric acid was highly hygroscopic and could hydrolyze phosphoric acid upon absorption of water. Moreover, polymeric acid-doped PBI was able to maintain the high proton conductivity at the operating temperatures over 200 °C and also to exhibit low gas permeability as well as excellent oxidative and thermal stabilities. Thus, polymeric acids can be used for synthesizing high-acid-doped PBI membranes. Xiao et al. [14] synthesized PBI polymers using polyphosphoric acid as both the polycondensation agent and the polymerization solvent, starting from tetraamino-biphenyl and dicarboxylic acids (Figure 15). After polymerization, the PBI solutions in polyphosphoric acid were directly cast into films at temperatures of 200–220 °C without isolation or re-dissolution of polymers. During the hydrolysis of the solvent from polyphosphoric acid to phosphoric acid, a transition from the solution state to gel state was observed. The resulting membranes with a desirable suite of physicochemical properties. The authors also demonstrated that such acid-doped PBI membranes through polyphosphoric acid possessed good mechanical properties. For example, at high phosphoric acid-doping levels, the average tensile strength and elongation at break were up to 3.5 MPa and 390%, respectively. As it is well-known, the proton conductivity of phosphoric acid-doped PBI membranes is closely dependent upon the external humidity [89]. Nevertheless, to avoid any external humidification is highly desired for high-temperature PEMFCs. The acid-doped PBI membranes made by the sol–gel process (Figure 15) exhibited a high acid-doping level of 32 mol of phosphoric acid per PBI repeat unit. Compared to conventional processes, this approach greatly improved the proton conductivity of PBI membranes, such as 0.01 S·cm⁻¹ at room temperature and 0.26 S·cm⁻¹ at 200 °C (Figure 16). Furthermore, the highest power output reached as high as 0.9 W·cm⁻² at an ambient pressure with a current density of 2.5 A·cm⁻².

Similarly, Li and coworkers [66] reported a thermally stable and organosoluble phenylindane-containing PBI membranes using polyphosphoric acid as both solvent and dehydrating agent (Figure 17). Compared to the pristine PBI, introduction of phenylindane acid into the PBI backbone disrupted close polymer chain packing, which not only greatly improved the PBI's solubility in polar aprotic solvents but also retained the good thermal stability. The synthesized acid-doped phenylindane-PBI membranes with an acid-doping level of 10.0 mol phosphoric acid per PBI repeat unit exhibited the highest proton conductivity of 0.061 S·cm⁻¹ at 180 °C. For fuel cell measurements, the highest power density for phenylindane-PBI membranes reached 0.36 W·cm⁻² in H₂/air at 180 °C when operated at atmospheric pressure with dry gases, which is higher than that of phosphoric acid-doped meta-PBI membranes under the similar testing conditions.

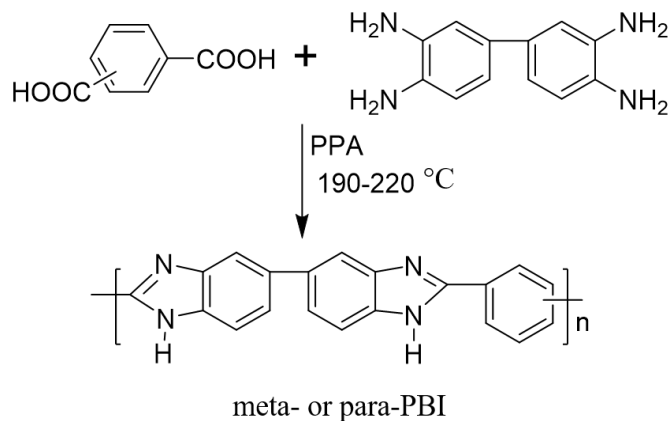


Figure 15. Synthesis of acid-doped PBI membranes in polyphosphoric acid. Reprinted with permission [14], 1996, Elsevier.

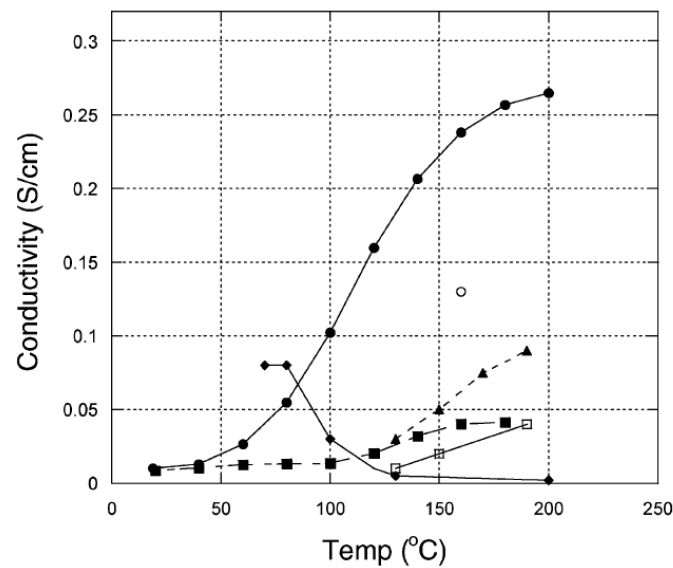


Figure 16. Proton conductivities of acid-doped PBI membranes from different processes: Membranes made from the sol-gel process (filled circles), conventional imbibing process (filled squares), conventional imbibing process (unfilled circle), imbibing from trifluoroacetic acid/phosphoric acid solvent (triangle), conventional imbibing process (unfilled squares), and sulfonated fluoropolymer (diamonds). Reprinted with permission [36], 2005, the American Chemical Society.

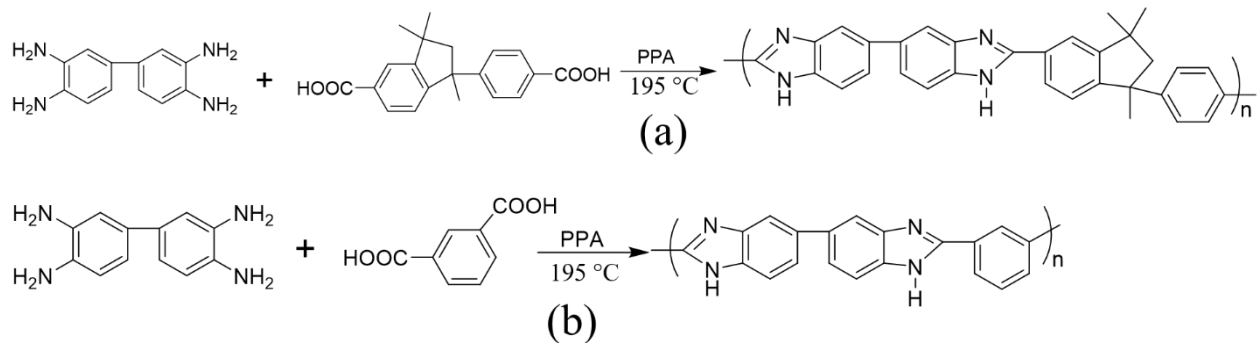


Figure 17. Synthesis of phenylindane-PBI (a) and meta-PBI (b) in polyphosphoric acid. Reprinted with permission [66], 2013, Elsevier.

To better understand the dependence of polyphosphoric acid upon the proton conductivity of PBI membranes, Leykin and coworkers [62] studied the interaction of polyphosphoric acid and PBI polymers with different chemical structures and found that absorption of polyphosphoric acid on PBI membranes during acid-doping was attributed to the three-stage isotherm sorption. Increase in concentration of the basic fragments in the repeating units of PBI does not necessarily increase the amount of absorbed polyphosphoric acid after doping. As a result of protonation of benzimidazole cycles, the developed positive charge impairs the basicity of the neighboring cycles. The basicity of PBI can be enhanced by introducing lengthy fragment-separating benzimidazole units in the main chain. Leaching phosphoric acid from the doped PBIs was virtually independent of the basicity of the polymers. To obtain doped PBI membranes with superior characteristics, two contradictory issues should be addressed, i.e., the high concentration of polyphosphoric acid in membranes and the good mechanical properties. Based on experimental results, acid-doped PBI membranes carried the ultimate tensile strength of 221 MPa and the elongation at break of 62%; the proton conductivity ranging from 0.025 to 0.052 S·cm⁻¹ was achieved at 180 °C.

6. Electrospun PBI Nanofiber Membranes for PEMs

In the above, a variety of acid-doped PBI membranes for use as PEMs have been produced mainly by the solution-casting technique. With recent development of the low-cost top-down electrospinning technique for fabrication of various continuous polymer nanofibers of broad polymers [90–95], electrospinning offers an alternative way for producing highly porous PBI nanofiber mats for PEMs. The schematic setup of an electrospinning process is shown in Figure 18, which consists of a spinneret connected to a polymer-solution pump, a high-voltage direct current (DC) power supply, and a fiber collector [96–99]. During a typical electrospinning process, a polymer-solution droplet is initiated and deformed to form a Taylor cone under the action of the induced electrostatic field. With increasing electrical field, the droplet is elongated until it overcomes its surface tension to emit a thin jet. The jet is further stretched and thinned in the electrostatic field until it loses stability in terms of vigorous jet whipping. After a variety of jet stabilities accompanying with fast solvent evaporation, the extremely thinned jet is dried and collected as a nonwoven nanofiber mat on the fiber collector. Figure 19 shows the typical nonwoven PBI nanofiber produced by electrospinning [100]. Back to the beginning of modern electrospinning in 1990s, Kim and Reneker [101] first produced continuous PBI nanofibers with the diameter of ~160–300 nm by electrospinning based on a PBI/dimethyl acetamide (DMAc) solution (with PBI and stabilizer LiCl mass concentrations of ~20 wt% and ~4 wt%, respectively). The resulting nonwoven PBI nanofiber mat was rinsed with a non-solvent (methanol) to remove the residual solvent (DMAc) and LiCl, followed by washing in sulfuric acid that was diluted to 50 wt% with deionized water to stabilize against shrinkage during heat treatment and to increase the mechanical strength. In recent years, nonwoven electrospun PBI nanofiber mats have been under growing investigation as promising PEMs for use in intermediate- and high-temperature PEMFCs [32,102–106]. For instance, the proton conductivity of phosphoric acid-doped nonwoven PBI nanofiber membranes (composited with polybenzoxazine-PBz) can reach as high as $0.17 \text{ S}\cdot\text{cm}^{-1}$ at $160 \text{ }^\circ\text{C}$ under anhydrous condition [32]. In this study, the PBz was introduced to the PBI nanofibers to serve as the crosslinking agent and also to enhance the formation of long range proton-conductive channels in the PBI membranes. The highly porous nonwoven PBI nanofiber mats with high specific surface area provided the advantage for fast, uniform acid-doping since liquid acids could quickly fill into the pores and diffuse into the PBI nanofibers, and the nanofibrous structures also provided ultrafast surface proton conduction. In addition, experimental results also showed that phytic acid-doped electrospun PBI nanofiber membranes exhibited much higher proton conductivity than Nafion[®] at low relative humidity [104]. To explore the mechanisms of proton conduct in acid-doped PBI nanofibers, Ibaraki et al. [104] measured the proton conductivity along the parallel and perpendicular directions of aligned PBI nanofiber membranes doped with phosphoric acid. They found the proton conductivity along the parallel direction was obviously higher than that along the perpendicular direction especially at low RHs (Figure 20). SEM-based microstructural analysis indicated that the higher proton conductivity was attributed to the proton hopping between phosphoric acid groups on the nanofiber surfaces. As a matter of fact, phosphoric acid groups can be easily aggregated at the nanofiber surfaces, which built up more effective proton conductive pathways along the fiber directions in the PBI nanofiber membranes. Muthuraja et al. [105] performed the comparative study of the proton conductivity of electrospun poly (aryl sulfone ether benzimidazole) (SO₂-OPBI) nanofiber membrane and its counterpart of dense solution-cast membranes, both of which were doped with phosphoric acid. It was found that the nanofiber membranes possessed a greatly increased proton conductivity ($0.0667 \text{ S}\cdot\text{cm}^{-1}$ at $160 \text{ }^\circ\text{C}$ and a doping level of 338 wt%) compared to that of the dense solution-cast membranes ($0.033 \text{ S}\cdot\text{cm}^{-1}$ at $160 \text{ }^\circ\text{C}$ and a doping level of 221 wt%), while both membranes showed very good oxidative and thermal stabilities. Clearly, the porous microstructures of PBI nanofiber mats provide more surface area and microscale pores for doping more acids, and thus more effective proton conduct pathways can be established. Recently Kallem et al. [106] systematically analyzed

the methodology of nanofiber-based PEMs and proposed aligned electrospun nanofibers for PEMFCs. Three types of conceptual nanofiber-based PEMs can be formulated, i.e., (a) proton conducting polymer supported by inert electrospun nanofibers, (b) inert polymer embedded with electrospun proton-conducting nanofibers, and (c) proton conducting polymer embedded with electrospun proton-conducting nanofibers. Acid-doped PBI nanofiber membranes can be classified as type (c) as both acid-doped PBI nanofibers and acid between nanofibers are proton conductive, which shows the great opportunity for developing high-performance PEMs for intermediate- and high-temperature PEMFCs. In addition, recent study also showed the promising conditions for PBI nanofiber fabrication, such as replacing the commonly used organic solvent DMAc by environmentally friendly and cheap ethanol/potassium hydroxide (ethanol/KOH) [107]. Expanding research investigations are expected in the near future for controllable PBI nanofiber fabrication and applications of PBI nanofiber PEMs for use in PEMFCs.

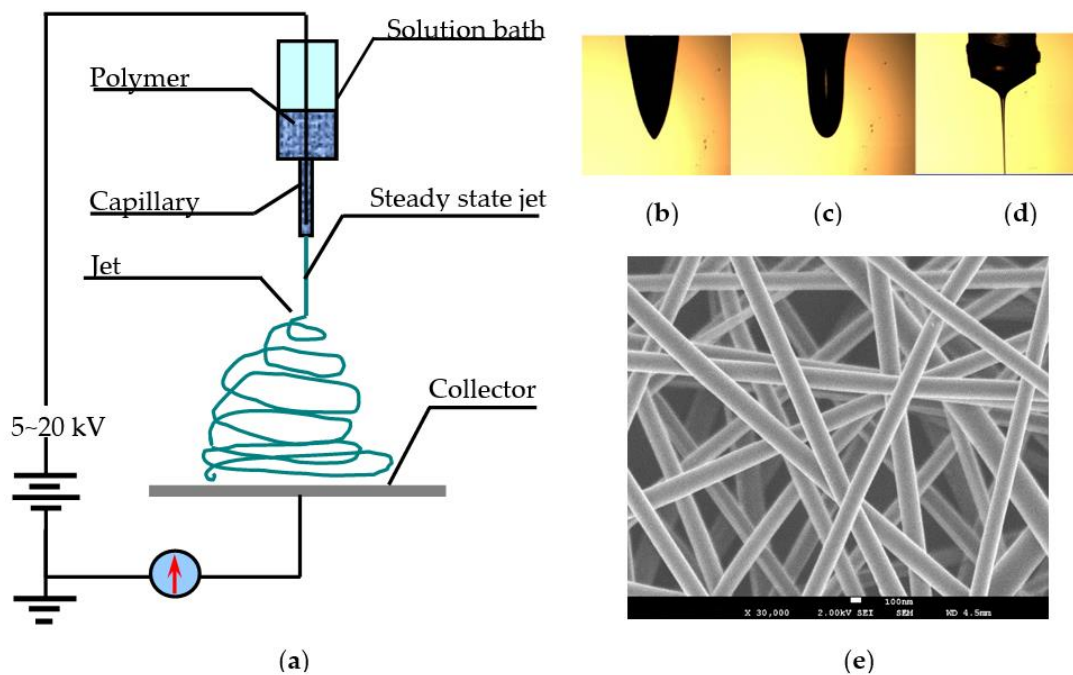


Figure 18. Electrospinning process for continuous nanofiber fabrication: (a) schematic electrospinning setup, (b) Taylor cone (deformed droplet in electrostatic field), (c) stretched droplet in electrostatic field, (d) straight jet in a stable electrospinning process, and (e) nonwoven continuous polyacrylonitrile (PAN) nanofibers collected on a fiber collector. Reprinted with permission [96], 2020, the American Institute of Physics.

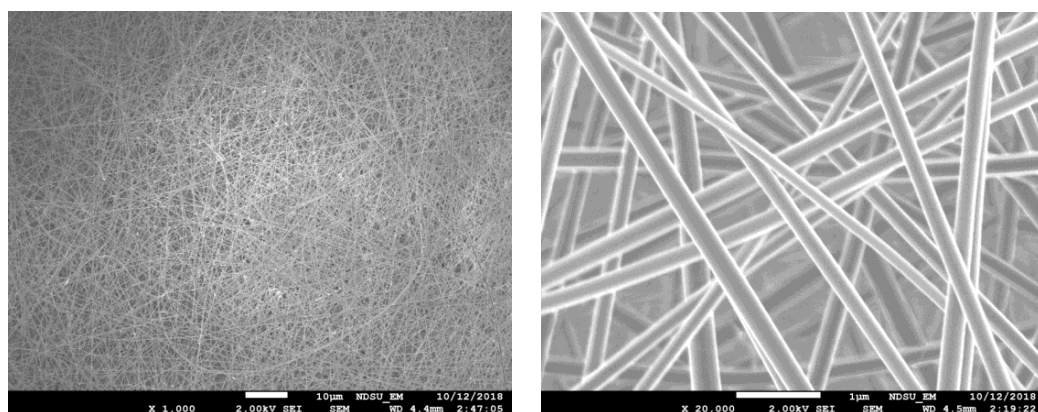


Figure 19. Low- and high-magnification ($\times 1000$ and $\times 20,000$) SEM micrographs of as-electrospun continuous monolithic PBI nanofibers with diameters of ~ 250 nm. Reprinted with permission [100], 2020, Wiley.

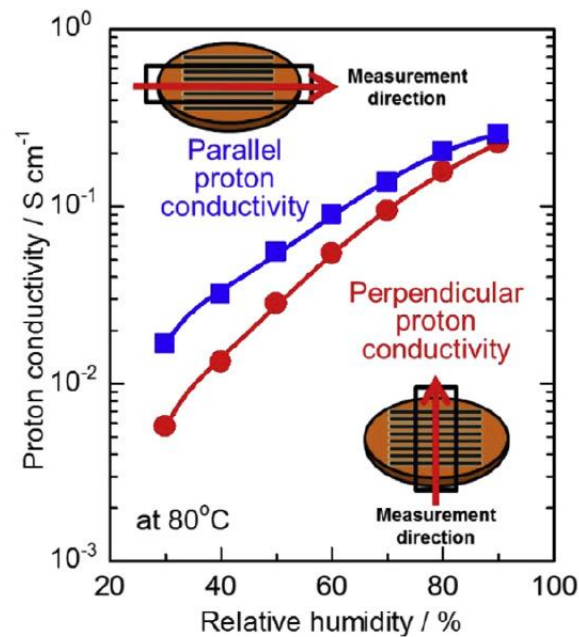


Figure 20. Variations of the proton conductivity with respect to varying HR at 80 °C (measured along the parallel and perpendicular directions of aligned PBI nanofiber membranes doped with phosphoric acid, respectively). Reprinted with permission [104], 2019, Elsevier.

7. Conclusions

PBI membranes have been under intensive investigation for over two decades for use in high-temperature PEMFCs. Integration of acid-doped PBI membranes into fuel cell devices is expected to grow rapidly. Compared to Nafion[®] and other membranes based on hydrated polymers, the operating temperatures of acid-doped PBI membranes are much higher, providing several advantages relating CO tolerance of catalyst layers, etc. Replacement of Nafion[®] membranes is considered as one of the technical challenges and opportunities for developing high-performance hydrogen fuel cells in the near future. Substantial efforts have been dedicated to the investigation on PBI membranes, which has led to breakthroughs for PEMFCs.

Focus has been made in this work on the mechanisms and technical approaches to modifications of PBI membranes as well as design, synthesis, and performances of acid-doped PBI membranes as PEMs. The literature review made in this study has confirmed that acid-doped PBI membranes play a crucial role in high-temperature PEMs for hydrogen fuel cells, with their capability of completely scrapping all humidification systems and high tolerance to impure fuels, particularly for hydrogen reformed from methane. Phosphoric, sulfuric, and polymeric acids have been considered as acid-doping agents for developing high-performance PBI-based PEMs with improved proton conductivities. Significance of controlling the dispersion and doping level of inorganic and organic acids on the proton conductivities of PBI membranes has also been discussed. To optimize the proton conductivity, designs of feasible technical approaches for effective interaction of inorganic or organic acids with PBI polymer structures are needed. In addition, advantages and drawbacks of these acids for acid-doped PBI membranes for achieving high proton conductivities have been addressed. Sulfonated PBI polymers have achieved similar proton conductivities by direct polymerization. Beyond proton conductivity and electrochemical performance, the mechanical properties of PBI membranes and relevant effects on acid-doping level and reaction time on structure and morphology have been addressed. Recent intensive research expands the already broad landscape of PBI membranes doped with a variety of acids, which deepens and broadens our outstanding of these high-performance functional membranes to greatly enhance the performance of PEMs. Finally, electrospinning technique provides a low-cost method to produce highly porous PBI nanofiber membranes with well

controlled thickness. These nanofibrous PBI membranes provide technical advantages for fast and high-load acid doping to achieve high proton conductivity. It can be concluded that the high-temperature PBIs provide a variety of technological opportunities to develop high-performance polymer-based PEMs for use in intermediate- and high-temperature PEMFCs for high-efficiency renewable energy conversion.

Author Contributions: X.-F.W. and T.A. conceived the paper, Z.Z. and X.-F.W. wrote the manuscript, and O.Z. and X.-F.W. revised the paper. All the authors have read, discussed and made comments to improve the manuscript, and agreed with submission of this manuscript for publication.

Funding: The U.S. Department of Energy (Award No. DE-EE008424), North Dakota (ND) Industrial Commission (Award No. R-036-45), ND EPSCoR (Award No. 0032106), ND Corn Utilization Council (Award No. FAR0032332), and ND Development Foundation (Award No. FAR0031220).

Institutional Review Board Statement: Not applicable.

Informed Consent Statement: Not applicable.

Data Availability Statement: All the data used in this paper are inclusively available in the cited journal papers.

Acknowledgments: The financial support of this research by the Office of Energy Efficiency and Renewable Energy (EERE) of the U.S. Department of Energy under the Advanced Manufacturing Office (Award no. DE-EE0008324) and the Renewable Energy Program of the Industrial Commission of North Dakota (Award no. R-036-45) is gratefully acknowledged. The views and opinions of authors expressed herein do not necessarily state or reflect those of the United States Government, the Industrial Commission of North Dakota, the EERC, or any agency thereof. The study at North Dakota State University (NDSU) is also sponsored by the ND EPSCoR (award no. FAR0032106), ND Corn Utilization Council (Award no. FAR0032332), and NDSU Development Foundation (Award no. FAR0031220).

Conflicts of Interest: The authors declare no conflict of interest.

References

1. Borup, R.; Meyers, J.; Pivovar, B.; Kim, Y.S.; Mukundan, R.; Garland, N.; Myers, D.; Wilson, M.; Garzon, F.; Wood, D.; et al. Scientific aspects of polymer electrolyte fuel cell durability and degradation. *Chem. Rev.* **2007**, *107*, 3904–3951. [[CrossRef](#)] [[PubMed](#)]
2. Zhan, Z.; Barnett, S.A. An octane-fueled solid oxide fuel cell. *Science* **2005**, *308*, 844–847. [[CrossRef](#)] [[PubMed](#)]
3. Steele, B.C.H.; Heinzel, A. Materials for fuel cell technologies. In *Materials for Sustainable Energy*; Dusastre, V., Ed.; Nature Publishing Group: London, UK, 2011; pp. 224–231. [[CrossRef](#)]
4. Wachsman, E.D.; Lee, K.T. Lowering the temperature of solid oxide fuel cells. *Science* **2011**, *334*, 935–939. [[CrossRef](#)] [[PubMed](#)]
5. Laberty-Robert, C.; Vallé, K.; Pereira, F.; Sanchez, C. Design and properties of functional hybrid organic–inorganic membranes for fuel cells. *Chem. Soc. Rev.* **2011**, *40*, 961–1005. [[CrossRef](#)] [[PubMed](#)]
6. Bose, S.; Kuila, T.; Bguyen, T.X.H.; Kim, N.H.; Lau, K.T.; Lee, J.H. Polymer membranes for high temperature proton exchange membrane fuel cell: Recent advances and challenges. *Prog. Polym. Sci.* **2011**, *36*, 813–843. [[CrossRef](#)]
7. Zhang, H.; Shen, P.K. Recent Development of polymer electrolyte membranes for fuel cells. *Chem. Rev.* **2012**, *112*, 2780–2832. [[CrossRef](#)]
8. Asensio, J.A.; Sánchez, E.M.; Gómez-Romero, P. Proton-conducting membranes based on benzimidazole polymers for high-temperature PEM fuel cells. A chemical quest. *Chem. Soc. Rev.* **2010**, *39*, 3210–3239. [[CrossRef](#)]
9. Li, Q.; He, R.; Jensen, J.O.; Bjerrum, N.J. Approaches and recent development of polymer electrolyte membranes for fuel cells operating above 100 °C. *Chem. Mater.* **2003**, *15*, 4896–4915. [[CrossRef](#)]
10. Li, Q.; He, R.; Jensen, J.O.; Bjerrum, N.J. PBI-based polymer membranes for high temperature fuel cells—Preparation, characterization and fuel cell demonstration. *Fuel Cells* **2004**, *4*, 147–159. [[CrossRef](#)]
11. Pan, C.; He, R.; Li, Q.; Jensen, J.O.; Bjerrum, N.J.; Hjulmand, H.A.; Jensen, A.B. Integration of high temperature PEM fuel cells with a methanol reformer. *J. Power Sources* **2005**, *145*, 392–398. [[CrossRef](#)]
12. Fujigaya, T.; Nakashima, N. Fuel cell electrocatalyst using polybenzimidazole-modified carbon nanotubes as support materials. *Adv. Mater.* **2013**, *25*, 1666–1681. [[CrossRef](#)] [[PubMed](#)]
13. Neburchilov, V.; Martin, J.; Wang, H.; Zhang, J. A review of polymer electrolyte membranes for direct methanol fuel cells. *J. Power Sources* **2007**, *169*, 221–238. [[CrossRef](#)]
14. Xiao, L.; Zhang, H.; Jana, T.; Scanlon, E.; Chen, R.; Choe, E.-W.; Ramanathan, L.S.; Yu, S.; Benicewicz, B.C. Synthesis and characterization of pyridine-based polybenzimidazoles for high temperature polymer electrolyte membrane fuel cell applications. *Fuel Cells* **2005**, *5*, 287–295. [[CrossRef](#)]

15. Wang, J.T.; Savinell, R.F.; Wainright, J.; Litt, M.; Yu, H. A H₂O₂ fuel cell using acid doped polybenzimidazole as polymer electrolyte. *Electrochim. Acta* **1996**, *41*, 193–197. [[CrossRef](#)]
16. Li, Q.; Jensen, J.O.; Savinell, R.F.; Bjerrum, N.J. High temperature proton exchange membranes based on polybenzimidazoles for fuel cells. *Prog. Polym. Sci.* **2009**, *34*, 449–477. [[CrossRef](#)]
17. Weber, J.; Kreuer, K.-D.; Maier, J.; Thomas, A. Proton Conductivity enhancement by nanostructural control of poly(benzimidazole)-phosphoric acid adducts. *Adv. Mater.* **2008**, *20*, 2595–2598. [[CrossRef](#)]
18. Wang, J.T.; Lin, W.F.; Weber, M.; Wasmus, S.; Savinell, R.F. Trimethoxymethane as an alternative fuel for a direct oxidation PBI polymer electrolyte fuel cell. *Electrochim. Acta* **1998**, *43*, 3821–3828. [[CrossRef](#)]
19. Lobato, J.; Cañizares, P.; Rodrigo, M.A.; Linares, J.J. PBI-based polymer electrolyte membranes fuel cells: Temperature effects on cell performance and catalyst stability. *Electrochim. Acta* **2007**, *52*, 3910–3920. [[CrossRef](#)]
20. Xing, B.; Savadogo, O. Hydrogen/oxygen polymer electrolyte membrane fuel cells (PEMFCs) based on alkaline-doped polybenzimidazole (PBI). *Electrochem. Commun.* **2000**, *2*, 697–702. [[CrossRef](#)]
21. Savadogo, O.; Varela, F.J.R. Low temperature direct propane polymer electrolyte membranes fuel cell (DPFC). *J. New Mater. Electrochem. Syst.* **2001**, *4*, 93–98.
22. Kawahara, M.; Morita, J.; Rikukawa, M.; Sanui, K.; Ogata, N. Synthesis and proton conductivity of thermally stable polymer electrolyte: Poly(benzimidazole) complexes with strong acid molecules. *Electrochim. Acta* **2000**, *45*, 1395–1398. [[CrossRef](#)]
23. Bouchet, R.; Miller, S.; Duclot, M.; Souquet, J.L. A thermodynamic approach to proton conductivity in acid-doped polybenzimidazole. *Solid State Ion.* **2001**, *145*, 69–78. [[CrossRef](#)]
24. Ma, Y.L.; Wainright, J.S.; Litt, M.H.; Savinell, R.F. Conductivity of PBI membranes for high-temperature polymer electrolyte fuel cells. *J. Electrochem. Soc.* **2004**, *151*, A8–A16. [[CrossRef](#)]
25. Baozhong, X.; Savadogo, O. The effect of acid doping on the conductivity of polybenzimidazole (PBI). *J. New Mater. Electrochem. Syst.* **1999**, *2*, 95–101.
26. Melchior, J.P.; Majer, G.; Kreuer, K.D. Why do proton conducting polybenzimidazole phosphoric acid membranes perform well in high-temperature PEM fuel cells? *Phys. Chem. Chem. Phys.* **2017**, *19*, 601–612. [[CrossRef](#)] [[PubMed](#)]
27. Herranz, D.; Escudero-Cid, R.; Montiel, M.; Palacio, C.; Fatás, E.; Ocón, P. Poly (vinyl alcohol) and poly (benzimidazole) blend membranes for high performance alkaline direct ethanol fuel cells. *Renew. Energy* **2018**, *127*, 883–895. [[CrossRef](#)]
28. Glipa, X.; Bonnet, B.; Mula, B.; Jones, D.J.; Rozière, J. Investigation of the conduction properties of phosphoric and sulfuric acid doped polybenzimidazole. *J. Mater. Chem.* **1999**, *9*, 3045–3049. [[CrossRef](#)]
29. Wainright, J.S.; Wang, J.T.; Weng, D.; Savinell, R.F.; Litt, M. Acid-doped polybenzimidazoles: A new polymer electrolyte. *J. Electrochem. Soc.* **1995**, *142*, L121–L123. [[CrossRef](#)]
30. Xu, H.; Chen, K.; Guo, X.; Fang, J.; Yin, J. Synthesis of novel sulfonated polybenzimidazole and preparation of cross-linked membranes for fuel cell application. *Polymer* **2007**, *48*, 5556–5564. [[CrossRef](#)]
31. Lee, H.S.; Roy, A.; Lane, O.; McGrath, J.E. Synthesis and characterization of poly(arylene ether sulfone)-b-polybenzimidazole copolymers for high temperature low humidity proton exchange membrane fuel cells. *Polymer* **2008**, *49*, 5387–5396. [[CrossRef](#)]
32. Li, H.Y.; Liu, Y.L. Polyelectrolyte composite membranes of polybenzimidazole and crosslinked polybenzimidazole-polybenzoxazine electrospun nanofibers for proton exchange membrane fuel cells. *J. Mater. Chem. A* **2013**, *1*, 1171–1178. [[CrossRef](#)]
33. Mader, J.A.; Benicewicz, B.C. Sulfonated polybenzimidazoles for high temperature PEM fuel cells. *Macromolecules* **2010**, *43*, 6706–6715. [[CrossRef](#)]
34. Berber, M.R.; Fujigaya, T.; Sasaki, K.; Nakashima, N. Remarkably durable high temperature polymer electrolyte fuel cell based on poly(vinylphosphonic acid)-doped polybenzimidazole. *Sci. Rep.* **2013**, *3*, 1764. [[CrossRef](#)]
35. Qingfeng, L.; Hjuler, H.A.; Hasiotis, C.; Kallitsis, J.K.; Kontoyannis, C.G.; Bjerrum, N.J. A quasi-direct methanol fuel cell system based on blend polymer membrane electrolytes. *Electrochem. Solid State Lett.* **2002**, *5*, A125–A128. [[CrossRef](#)]
36. Xiao, L.; Zhang, H.; Scanlon, E.; Ramanathan, L.S.; Choe, E.W.; Rogers, D.; Apple, T.; Benicewicz, B.C. High-temperature polybenzimidazole fuel cell membranes via a sol–gel process. *Chem. Mater.* **2005**, *17*, 5328–5333. [[CrossRef](#)]
37. He, R.; Li, Q.; Xiao, G.; Bjerrum, N.J. Proton conductivity of phosphoric acid doped polybenzimidazole and its composites with inorganic proton conductors. *J. Membr. Sci.* **2003**, *226*, 169–184. [[CrossRef](#)]
38. Staiti, P.; Minutoli, M.; Hocevar, S. Membranes based on phosphotungstic acid and polybenzimidazole for fuel cell application. *J. Power Sources* **2000**, *90*, 231–235. [[CrossRef](#)]
39. Staiti, P.; Minutoli, M. Influence of composition and acid treatment on proton conduction of composite polybenzimidazole membranes. *J. Power Sources* **2001**, *94*, 9–13. [[CrossRef](#)]
40. Wang, J.T.W.; Hsu, S.L.C. Enhanced high-temperature polymer electrolyte membrane for fuel cells based on polybenzimidazole and ionic liquids. *Electrochim. Acta* **2011**, *56*, 2842–2846. [[CrossRef](#)]
41. Shabanikia, A.; Javanbakht, M.; Amoli, H.S.; Hooshyari, K.; Enhessari, M. Polybenzimidazole/strontium cerate nanocomposites with enhanced proton conductivity for proton exchange membrane fuel cells operating at high temperature. *Electrochim. Acta* **2015**, *154*, 370–378. [[CrossRef](#)]
42. Lin, J.; Yan, X.; He, G.; Chen, W.; Zhen, D.; Li, T.; Ma, L.; Wu, X. Thermoplastic interpenetrating polymer networks based on polybenzimidazole and poly (1, 2-dimethyl-3-allylimidazolium) for anion exchange membranes. *Electrochim. Acta* **2017**, *257*, 9–19. [[CrossRef](#)]

43. Krishnan, N.N.; Lee, H.J.; Kim, H.J.; Kim, J.Y.; Hwang, I.; Jang, J.H.; Cho, E.A.; Kim, S.K.; Henkensmeier, D.; Hong, S.A.; et al. Sulfonated poly(ether sulfone)/sulfonated polybenzimidazole blend membrane for fuel cell applications. *Eur. Polym. J.* **2010**, *46*, 1633–1641. [[CrossRef](#)]
44. Hou, H.; Sun, G.; He, R.; Sun, B.; Jin, W.; Liu, H.; Xin, Q. Alkali doped polybenzimidazole membrane for alkaline direct methanol fuel cell. *Int. J. Hydrogen Energy* **2008**, *33*, 7172–7176. [[CrossRef](#)]
45. Wannek, C.; Konradi, I.; Mergel, J.; Lehnert, W. Redistribution of phosphoric acid in membrane electrode assemblies for high-temperature polymer electrolyte fuel cells. *Int. J. Hydrogen Energy* **2009**, *34*, 9479–9485. [[CrossRef](#)]
46. Sun, P.; Li, Z.; Dong, F.; Wang, S.; Yin, X.; Wang, Y. High temperature proton exchange membranes based on cerium sulfophenyl phosphate doped polybenzimidazole by end-group protection and hot-pressing method. *Int. J. Hydrogen Energy* **2017**, *42*, 486–495. [[CrossRef](#)]
47. Üregen, N.; Pehlivanoglu, K.; Özdemir, Y.; Devrim, Y. Development of polybenzimidazole/graphene oxide composite membranes for high temperature PEM fuel cells. *Int. J. Hydrogen Energy* **2017**, *42*, 2636–2647. [[CrossRef](#)]
48. Özdemir, Y.; Üregen, N.; Devrim, Y. Polybenzimidazole based nanocomposite membranes with enhanced proton conductivity for high temperature PEM fuel cells. *Int. J. Hydrogen Energy* **2017**, *42*, 2648–2657. [[CrossRef](#)]
49. Asensio, J.A.; Borrós, S.; Gómez-Romero, P. Polymer electrolyte fuel cells based on phosphoric acid-impregnated poly(2,5-benzimidazole) membranes. *J. Electrochem. Soc.* **2004**, *151*, A304–A310. [[CrossRef](#)]
50. Huang, C.W.; Hsu, C.H.; Kuo, P.L.; Hsieh, C.T.; Teng, H. Mesoporous carbon spheres grafted with carbon nanofibers for high-rate electric double layer capacitors. *Carbon* **2011**, *49*, 895–903. [[CrossRef](#)]
51. Sun, P.; Li, Z.; Wang, S.; Yin, X. Performance enhancement of polybenzimidazole based high temperature proton exchange membranes with multifunctional crosslinker and highly sulfonated polyaniline. *J. Membr. Sci.* **2018**, *549*, 660–669. [[CrossRef](#)]
52. Krishnan, N.N.; Lee, S.; Ghorpade, R.V.; Konovalova, A.; Jang, J.H.; Kim, H.J.; Han, J.; Henkensmeier, D.; Han, H. Polybenzimidazole (PBI-OO) based composite membranes using sulfophenylated TiO₂ as both filler and crosslinker, and their use in the HT-PEM fuel cell. *J. Membr. Sci.* **2018**, *560*, 11–20. [[CrossRef](#)]
53. Li, S.; Zhu, X.; Liu, D.; Sun, F. A highly durable long side-chain polybenzimidazole anion exchange membrane for AEMFC. *J. Membr. Sci.* **2018**, *546*, 15–21. [[CrossRef](#)]
54. Krishnan, N.N.; Joseph, D.; Duong, N.M.H.; Konovalova, A.; Jang, J.H.; Kim, H.J.; Nam, S.W.; Henkensmeier, D. Phosphoric acid doped crosslinked polybenzimidazole (PBI-OO) blend membranes for high temperature polymer electrolyte fuel cells. *J. Membr. Sci.* **2017**, *544*, 416–424. [[CrossRef](#)]
55. Fang, J.; Lin, X.; Cai, D.; He, N.; Zhao, J. Preparation and characterization of novel pyridine-containing polybenzimidazole membrane for high temperature proton exchange membrane fuel cells. *J. Membr. Sci.* **2016**, *502*, 29–36. [[CrossRef](#)]
56. Chen, J.C.; Chen, P.Y.; Liu, Y.C.; Chen, K.H. Polybenzimidazoles containing bulky substituents and ether linkages for high-temperature proton exchange membrane fuel cell applications. *J. Membr. Sci.* **2016**, *513*, 270–279. [[CrossRef](#)]
57. Ngamsantivongsa, P.; Lin, H.L.; Leon Yu, T. Properties and fuel cell applications of polybenzimidazole and ethyl phosphoric acid grafted polybenzimidazole blend membranes. *J. Membr. Sci.* **2015**, *491*, 10–21. [[CrossRef](#)]
58. Yang, J.; Xu, Y.; Zhou, L.; Che, Q.; He, R.; Li, Q. Hydroxyl pyridine containing polybenzimidazole membranes for proton exchange membrane fuel cells. *J. Membr. Sci.* **2013**, *446*, 318–325. [[CrossRef](#)]
59. Chang, Y.N.; Lai, J.Y.; Liu, Y.L. Polybenzimidazole (PBI)-functionalized silica nanoparticles modified PBI nanocomposite membranes for proton exchange membranes fuel cells. *J. Membr. Sci.* **2012**, *403–404*, 1–7. [[CrossRef](#)]
60. Shen, C.H.; Hsu, S.L.C.; Bulycheva, E.; Belomoina, N. Polybenzimidazole/1H-imidazole-4-sulfonic acid hybrid membranes for high-temperature proton exchange membranes fuel cells. *J. Membr. Sci.* **2012**, *399–400*, 11–15. [[CrossRef](#)]
61. Plackett, D.; Siu, A.; Li, Q.; Pan, C.; Jensen, J.O.; Nielsen, S.F.; Permyakova, A.A.; Bjerrum, N.J. High-temperature proton exchange membranes based on polybenzimidazole and clay composites for fuel cells. *J. Membr. Sci.* **2011**, *383*, 78–87. [[CrossRef](#)]
62. Leykin, A.Y.; Askadskii, A.A.; Vasilev, V.G.; Rusanov, A.L. Dependence of some properties of phosphoric acid doped PBIs on their chemical structure. *J. Membr. Sci.* **2010**, *347*, 69–74. [[CrossRef](#)]
63. Hu, M.; Ni, J.; Zhang, B.; Neelakandan, S.; Wang, L. Crosslinked polybenzimidazoles containing branching structure as membrane materials with excellent cell performance and durability for fuel cell applications. *J. Power Sources* **2018**, *389*, 222–229. [[CrossRef](#)]
64. Li, X.; Ma, H.; Shen, Y.; Hu, W.; Jiang, Z.; Liu, B.; Guiver, M.G. Dimensionally-stable phosphoric acid-doped polybenzimidazoles for high-temperature proton exchange membrane fuel cells. *J. Power Sources* **2016**, *336*, 391–400. [[CrossRef](#)]
65. Mack, F.; Heissler, S.; Laukenmann, R.; Zeis, R. Phosphoric acid distribution and its impact on the performance of polybenzimidazole membranes. *J. Power Sources* **2014**, *270*, 627–633. [[CrossRef](#)]
66. Li, X.; Chen, X.; Benicewicz, B.C. Synthesis and properties of phenylindane-containing polybenzimidazole (PBI) for high-temperature polymer electrolyte membrane fuel cells (PEMFCs). *J. Power Sources* **2013**, *243*, 796–804. [[CrossRef](#)]
67. Van de Ven, E.; Chairuna, A.; Merle, G.; Benito, S.P.; Borneman, Z.; Nijmeijer, K. Ionic liquid doped polybenzimidazole membranes for high temperature Proton Exchange Membrane fuel cell applications. *J. Power Sources* **2013**, *222*, 202–209. [[CrossRef](#)]
68. Henkensmeier, D.; Kim, H.J.; Lee, H.J.; Lee, D.H.; Oh, I.H.; Hong, S.A.; Nam, S.W.; Lim, T.H. Polybenzimidazolium-based solid electrolytes. *Macromol. Mater. Eng.* **2011**, *296*, 899–908. [[CrossRef](#)]
69. Hou, H.; Sun, G.; He, R.; Wu, Z.; Sun, B. Alkali doped polybenzimidazole membrane for high performance alkaline direct ethanol fuel cell. *J. Power Sources* **2008**, *182*, 95–99. [[CrossRef](#)]

70. An, L.; Zeng, L.; Zhao, T.S. An alkaline direct ethylene glycol fuel cell with an alkali-doped polybenzimidazole membrane. *Int. J. Hydrogen Energy* **2013**, *38*, 10602–10606. [[CrossRef](#)]
71. Hou, H.; Wang, S.; Jiang, Q.; Jin, W.; Jiang, L.; Sun, G. Durability study of KOH doped polybenzimidazole membrane for air-breathing alkaline direct ethanol fuel cell. *J. Power Sources* **2011**, *196*, 3244–3248. [[CrossRef](#)]
72. Peron, J.; Ruiz, E.; Jones, D.J.; Rozière, J. Solution sulfonation of a novel polybenzimidazole: A proton electrolyte for fuel cell application. *J. Membr. Sci.* **2008**, *314*, 247–256. [[CrossRef](#)]
73. Ariza, M.J.; Jones, D.J.; Rozière, J. Role of post-sulfonation thermal treatment in conducting and thermal properties of sulfuric acid sulfonated poly(benzimidazole) membranes. *Desalination* **2002**, *147*, 183–189. [[CrossRef](#)]
74. Staiti, P.; Lufitano, F.; Aricò, A.S.; Passalacqua, E.; Antonucci, V. Sulfonated polybenzimidazole membranes—preparation and physico-chemical characterization. *J. Membr. Sci.* **2001**, *188*, 71–78. [[CrossRef](#)]
75. Glipta, X.; Haddad, M.E.; Jones, D.J.; Rozière, J. Synthesis and characterisation of sulfonated polybenzimidazole: A highly conducting proton exchange polymer. *Solid State Ion.* **1997**, *97*, 323–331. [[CrossRef](#)]
76. Asensio, J.A.; Borrós, S.; Gómez-Romero, P. Sulfonated poly(2,5-benzimidazole) (SABPBI) impregnated with phosphoric acid as proton conducting membranes for polymer electrolyte fuel cells. *Electrochim. Acta* **2004**, *49*, 4461–4466. [[CrossRef](#)]
77. Wanek, C.; Lehnert, W.; Mergel, J. Membrane electrode assemblies for high-temperature polymer electrolyte fuel cells based on poly(2,5-benzimidazole) membranes with phosphoric acid impregnation via the catalyst layers. *J. Power Sources* **2009**, *192*, 258–266. [[CrossRef](#)]
78. Pu, H.; Liu, L.; Chang, Z.; Yuan, J. Organic/inorganic composite membranes based on polybenzimidazole and nano-SiO₂. *Electrochim. Acta* **2009**, *54*, 7536–7541. [[CrossRef](#)]
79. Chee, W.K.; Lim, H.N.; Huang, N.M.; Harrison, I. Nanocomposites of graphene/polymers: A review. *RSC Adv.* **2015**, *5*, 68014–68051. [[CrossRef](#)]
80. Qian, Y.; Lan, Y.; Xu, J.; Ye, F.; Dai, S. Fabrication of polyimide-based nanocomposites containing functionalized graphene oxide nanosheets by in-situ polymerization and their properties. *Appl. Surf. Sci.* **2014**, *314*, 991–999. [[CrossRef](#)]
81. Gao, W.; Alemany, L.B.; Ci, L.; Ajayan, P.M. New insights into the structure and reduction of graphite oxide. *Nat. Chem.* **2009**, *1*, 403–409. [[CrossRef](#)]
82. Xu, C.; Cao, Y.; Kumer, R.; Wu, X.; Wang, X.; Scott, K. A polybenzimidazole/sulfonated graphite oxide composite membrane for high temperature polymer electrolyte membrane fuel cells. *J. Mater. Chem.* **2011**, *21*, 11359–11364. [[CrossRef](#)]
83. He, R.; Li, Q.; Bach, A.; Jensen, J.O.; Bjerrum, N.J. Physicochemical properties of phosphoric acid doped polybenzimidazole membranes for fuel cells. *J. Membr. Sci.* **2006**, *277*, 38–45. [[CrossRef](#)]
84. Bae, J.M.; Honma, I.; Murata, M.; Yamamoto, T.; Rikukawa, M.; Ogata, N. Properties of selected sulfonated polymers as proton-conducting electrolytes for polymer electrolyte fuel cells. *Solid State Ion.* **2002**, *147*, 189–194. [[CrossRef](#)]
85. Asensio, J.A.; Borrós, S.; Gómez-Romero, P. Proton-conducting polymers based on benzimidazoles and sulfonated benzimidazoles. *J. Polym. Sci. Pol. Chem.* **2002**, *40*, 3703–3710. [[CrossRef](#)]
86. Wu, X.; Scott, K. A H₂SO₄ Loaded polybenzimidazole (PBI) membrane for high temperature PEMFC. *Fuel Cells* **2012**, *12*, 583–588. [[CrossRef](#)]
87. Vogel, H.; Marvel, C.S. Polybenzimidazoles, new thermally stable polymers. *J. Polym. Sci.* **1961**, *50*, 511–539. [[CrossRef](#)]
88. Makoto, K.; Osamu, O.; Ichiro, Y. Phosphorus nuclear magnetic resonance in polyphosphates and determination of their hydrolysis rate constants. *Bull. Chem. Soc. Jpn.* **1970**, *43*, 3705–3710. [[CrossRef](#)]
89. Schechter, A.; Savinell, R.F. Imidazole and 1-methyl imidazole in phosphoric acid doped polybenzimidazole, electrolyte for fuel cells. *Solid State Ion.* **2002**, *147*, 181–187. [[CrossRef](#)]
90. Reneker, D.H.; Chun, I. Nanometre diameter fibres of polymer, produced by electrospinning. *Nanotechnology* **1996**, *7*, 216–223. [[CrossRef](#)]
91. Reneker, R.H.; Yarin, A.L.; Zussman, E.; Xu, H. Electrospinning of nanofibers from polymer solutions and melts. *Adv. Appl. Mech.* **2007**, *41*, 43–195.
92. Reneker, D.H.; Yarin, A.L. Electrospinning jets and polymer nanofibers. *Polymer* **2008**, *49*, 2387–2425. [[CrossRef](#)]
93. Dzenis, Y. Spinning continuous fibers for nanotechnology. *Science* **2004**, *304*, 1917–1919. [[CrossRef](#)] [[PubMed](#)]
94. Li, D.; Xia, Y.N. Electrospinning of nanofibers: Reinventing the wheel? *Adv. Mater.* **2004**, *16*, 1151–1170. [[CrossRef](#)]
95. Lauricella, M.; Succi, S.; Zussman, E.; Pisignano, D.; Yarin, A.L. Models of polymer solutions in electrified jets and solution blowing. *Rev. Modern Phys.* **2020**, *92*, 035004. [[CrossRef](#)]
96. Wu, X.F.; Zhou, Z.; Zhobolko, O.; Jenniges, J.J.; Baatz, B.; Ahmadi, M.; Chen, J. Critical condition of electrohydrodynamic jetting from a polymer-solution droplet on a conductive wire. *J. Appl. Phys.* **2020**, *127*, 054303. [[CrossRef](#)]
97. Zhou, Z.; Wu, X.F.; Gao, X.; Jiang, L.; Zhao, Y.; Fong, H. Parameter dependence of conic angle of nanofibers during electrospinning. *J. Phys. D Appl. Phys.* **2011**, *44*, 435401. [[CrossRef](#)]
98. Wu, X.F.; Zhou, Z.; Rahman, A.; Bedarkar, A. Mechanical property of continuous nanofibers: Characterization and mechaics. In *Nanostructures: Properties, Production Methods and Applications*; Dong, Y., Ed.; Nova Scientific Publisher: New York, NY, USA, 2013; pp. 247–285.
99. Wu, X.F.; Zhobolko, O.; Zhou, Z.; Rahman, A. Electrospun nanofibers for interfacial toughening and damage self-healing of polymer composites and surface coatings. In *Electrospun Polymers and Composites*; Dong, Y., Baji, A., Ramakrishna, S., Eds.; Elsevier: New York, NY, USA, 2020; pp. 315–359.

100. Zholobko, O.; Wu, X.F.; Zhou, Z.; Aulich, T.; Thakare, J.; Hurley, J. A comparative experimental study of the hygroscopic and mechanical behaviors of electrospun nanofiber membranes and solution-cast films of polybenzimidazole. *J. Appl. Polym. Sci.* **2020**, *137*, 49639. [[CrossRef](#)]
101. Kim, J.S.; Reneker, D.H. Polybenzimidazole nanofiber produced by electrospinning. *Polym. Eng. Sci.* **1999**, *39*, 849–854. [[CrossRef](#)]
102. Weber, J. Nanostructured poly(benzimidazole): From mesoporous network to nanofibers. *ChemSusChem* **2010**, *3*, 181–187. [[CrossRef](#)]
103. Jahangiri, S.; Aravi, I.; Şanlı, L.I.; Menceloğlu, Y.Z.; Özden-Yenigün, E. Fabrication and optimization of proton conductive polybenzimidazole electrospun nanofiber membranes. *Polym. Adv. Technol.* **2018**, *29*, 594–602. [[CrossRef](#)]
104. Ibaraki, T.; Tanaka, M.; Kawakami, H. Fast surface proton conduction on acid-doped polymer nanofibers in polymer electrolyte composite membranes. *Electrochim. Acta* **2019**, *296*, 1042–1048. [[CrossRef](#)]
105. Muthuraja, P.; Prakash, S.; Shanmugam, V.M.; Manisankar, P. Stable nanofibrous poly(aryl sulfone ether benzimidazole) membrane with high conductivity for high temperature PEM fuel cells. *Solid State Ion.* **2018**, *317*, 201–209. [[CrossRef](#)]
106. Kallem, P.; Yanar, N.; Choi, H. Nanofiber-based proton exchange membranes: Development of aligned electrospun nanofibers for polymer electrolyte fuel cell applications. *ACS Sustain. Chem. Eng.* **2019**, *7*, 1808–1825. [[CrossRef](#)]
107. Penchev, H.; Ublekov, F.; Budurova, D.; Sinigersky, V. Novel electrospun polybenzimidazole fibers and yarns from ethanol/potassium hydroxide solution. *Mater. Lett.* **2017**, *187*, 89–93. [[CrossRef](#)]